Macromolecules

pubs.acs.org/Macromolecules Article

Controlling Mechanical Properties of Poly(methacrylic acid) Multilayer Hydrogels via Hydrogel Internal Architecture

Maksim Dolmat,[§] Veronika Kozlovskaya,[§] John F. Ankner,* and Eugenia Kharlampieva*

Cite This: https://doi.org/10.1021/acs.macromol.3c01253 Read Online

ACCESS | Metrics & More | Article Recommendations | Supporting Information

ABSTRACT: Hydrogel materials are crucial in many applications due to their versatility and ability to mimic biological tissues. While manipulating bulk hydrogel cross-link density, polymer content, chemical composition, and microporosity has been a main approach to controlling hydrogel rigidity, altering the internal organization of hydrogel materials through chain intermixing and stratification can bring finer control over hydrogel properties, including mechanical responses. We report on altering the mechanical properties of ultrathin poly(methacrylic acid) (PMAA) multilayer hydrogels by controlling the internal organization of the PMAA network. PMAA multilayer hydrogels were synthesized by cross-linking PMAA layers in poly(*N*-vinylpyrrolidone) (PVPON)/PMAA hydrogen-bonded multilayer templates prepared by dipped or spin-assisted (SA) layer-by-layer assembly using sacrificial PVPON interlayers with molecular weights of 40,000 or 280,000 g mol^{-1}. The effect of PVPON molecular weight on PMAA hydrogel stratification and network swelling and hydration was assessed by *in situ* spectroscopic ellipsometry and neutron reflectometry (NR). In a new NR modeling of polymer intermixing, we have inferred nanoscopic structure and water distribution within the ultrathin-layered films from measured continuum neutron scattering length density (SLD) and related those to the mechanical properties of the hydrogel films. We have found that hydrogel swelling, the number of water molecules associated with the swollen hydrogel, and water density within the SA PMAA hydrogels can be controlled by choosing low- or high-M_w PVPON. While cross-link densities determined by ATR-FTIR were similar, greater swelling and hydration at pH > 5 were observed for SA PMAA hydrogels synthesized using higher-M_w PVPON. The enhanced swelling of these SA hydrogels resulted in softening with a lower Young's modulus at pH > 5 as measured by colloidal probe atomic force microscopy (AFM). The effect of PMAA layer intermixing on hydrogel mechanical properties was also compared for dipped and SA (PMAA) multilayer hydrogels of similar thickness and cross-linking degree. Despite similar values of gigapascal-range Young's modulus for dry PMAA multilayer hydrogel films, an almost twice greater softening of the SA (PMAA) hydrogel compared to that prepared by dipping was observed, with Young's modulus values decreasing to tens of megapascals in solution at pH > 5. Our study demonstrates that, unlike simply changing bulk hydrogel cross-link density, programming polymer network architecture via controlling the nanostructured organization of SA PMAA hydrogels enables selective modulation of the cross-link density within hydrogel strata. Control of polymer chain intermixing through hydrogel stratification offers a framework for synthesizing materials with finely tuned hydrogel internal structures, enabling precise control of such physical properties as the internal architecture, hydrogel swelling, surface morphology, and mechanical response, which are critical for the application of these materials in sensing, drug delivery, and tissue engineering.

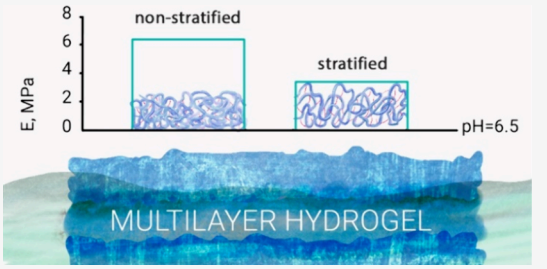

INTRODUCTION

Hydrogels are three-dimensional, hydrophilic polymer networks capable of absorbing large quantities of water or biological fluids and have become prominent in sensing, drug delivery, and tissue engineering applications due to their versatility and ability to mimic biological tissues.[1−6] Reversible volume-phase transitions in response to external stimuli can be used to control hydrogel properties for specific applications precisely.[7−11] Based on the classic Flory−Rehner model, the network volume transition is controlled by the expansive entropy forces associated with polymer−solvent mixing and the retractive elastic contribution of polymer chains.[12] The pH-regulated acid−base equilibrium controls volume change in ionic networks: Entropy is increased due to the dissociation of charges, while charged macromolecule chains lead to network swelling, which decreases the entropy of polymer chains.[13]

Controlling hydrogel mechanical properties is essential for regulating tissue growth, cell adhesion, gene expression, and fabricating effective, flexible sensors.[14−16] Manipulating hydro-

Received: June 26, 2023
Revised: September 7, 2023

gel cross-link density, polymer content, and chemical composition has been a main approach to adjusting hydrogel rigidity.[17−21] In addition, varying hydrogel microporosity via solvent casting/particle leaching,[22] electrospinning,[23] freeze-drying,[24] and gas foaming[25] has been shown to affect stiffness, swelling, and solute transport in bulk hydrogels.[2,26−29] For example, reducing hydrogel porosity by increasing the concentration of alginate in methacrylated gelatin resulted in a stiffer and more compact alginate-based hydrogel.[29]

Conversely, controlling the internal architecture of hydrogels on the nanoscale by varying chain arrangements and, subsequently, the free volume represents a new approach to synthesizing hydrogels with precisely controlled mechanical properties. For instance, step-polymerized poly(ethylene glycol)-based hydrogels showed enhanced tensile toughness, ductility, and shear strain to yield compared to chain-polymerized gels, suggesting that greater homogeneity enhances mechanical characteristics.[30] Also, by stretching an alginate/polyacrylamide bulk hydrogel to 300% of its initial length in one direction followed by secondary cross-linking, stiffness was shown to increase 64-fold compared to the unstretched hydrogel.[31] Zarket and Raghavan demonstrated that a cross-linked alginate gel exhibits different mechanical responses to compression when its onion-like shell comprises layers with different chemical compositions.[32] Another study used self-assemblies of synthetic colloids made of amorphous core and radial crystalline ribbons to obtain hydrogels through colloid−colloid interpenetration.[33] Extension-softening and compression-stiffening mechanical responses that mimic biological tissues were observed by controlling the interpenetration of these densely packed colloids.[33] Moreover, hierarchically structured anisotropic hydrogels of poly(vinyl alcohol) (PVA) nanofibrils obtained through freezing and salting out of PVA solution demonstrated a two- to fourfold improvement in strength and toughness, compared to a nonfibril chemically cross-linked PVA hydrogel.[34]

Ultrathin nanostructured multilayer hydrogels have been synthesized using layer-by-layer (LbL) assembly of polymers at surfaces.[35] The LbL technique enables precise control over the polymer multilayer composition, thickness, and physical properties at the nanoscale. The internal architecture of the polymer multilayer films has been shown to depend on interactions between the polymers,[36−38] polymer deposition method,[39,40] and polymer adsorption conditions[41,42] affecting the properties of the polymer multilayer material. Polymer molecular weight has been found to be a significant factor in regulating the structural organization of polyelectrolyte multilayers[43,44] and multilayer thickness,[45] roughness,[39,46] swelling,[47] mechanical properties,[48] and degradation.[39,49]

The effect of the internal organization of polymer multilayers on their properties has been explored using neutron reflectometry (NR) to determine layer density distribution within thin (ca. 100 nm) multilayer coatings by utilizing deuterated and protiated polymers and/or deuterated solvents.[50−52] Sukhishvili and colleagues investigated the impact of a competing solvent, DMSO, on the internal structure of hydrogen-bonded poly(methacrylic acid)/poly(*N*-vinylpyrrolidone) (PMAA/PVPON) during film assembly and found that LbL films experienced enhanced chain intermixing with increasing concentration of DMSO in the deposition solutions.[36] Willott and colleagues confirmed the formation of asymmetric LbL multilayer membranes containing distinct top poly(allylamine) (PAH)/poly(acrylic acid) (PAA) or PAH/Nafion and bottom poly(styrenesulfonate) (PSS)/(PAH) stacks.[53] Importantly, NR demonstrated that the reduced hydration of the PAH/Nafion stack makes the membrane denser and, consequently, more selective when compared to (PAH/PAA)-capped or symmetric (PSS/PAH) membranes.[53] By observing the M_w-dependent disintegration behavior of spin-assisted (SA) LbL linear poly(ethylene imine)(PEI)/PMAA films, with M_w of PMAA ranging from 15 to 226 kDa, NR provided fundamental insight into a pH-dependent chain- and structural-level behavior in (PEI/PMAA) multilayer films.[49] For instance, when subjected to pH 2, multilayers exhibited surface erosion or burst dissolution when films were made with high-M_w PMAA or low-M_w PMAA chains, respectively.[49]

Using NR, we demonstrated that the degree of pH-induced swelling of PMAA multilayer hydrogels could be controlled by regulating their internal structure from well-stratified to highly intermixed by varying assembly conditions (dipped versus SA).[44] Well-stratified hydrogels exhibited a dramatic 10-fold increase in thickness when transitioned between pH 5 and 7.5, compared to the twofold swelling observed in less-stratified dipped multilayer hydrogels, and maintained their stratification when exposed to solutions at various pH values.[44] The SA LbL assembly[54,55] resulted in polymer loops and tails being deposited in a mobility-limited "frozen" state without much intermixing with the neighboring layers, yielding a highly stratified cross-linked network.[44] These loops and entanglements expand at high pH, providing a free volume for swelling.

In contrast, polymer chains are more interdiffused in the dipped films, because of chain exchange during assembly. These chain entanglements decrease the free volume in the dipped hydrogels, significantly constraining hydrogel swelling.[44] We also showed that thickness, surface microstructure, and internal organization of the as-deposited hydrogen-bonded (PMAA/PVPON) multilayers and the corresponding (PMAA) multilayer hydrogels are strongly influenced by PVPON molecular weight.[56] Finally, we found that pH-induced swelling of a stratified SA PMAA multilayer hydrogel did not significantly disturb internal stratification at pH 7 compared to that for the dipped multilayer hydrogel.[40]

Based on this previous work, we hypothesize that chain entanglement or stratification of polymer layers should manifest in different mechanical properties of dipped and SA PMAA hydrogels in the hydrogel collapsed (pH 5) and swollen (pH > 5) states. We also hypothesize that increasing the molecular weight of the sacrificial binder, PVPON, during PMAA hydrogel assembly may result in softening in the (PMAA) hydrogel at pH > 6.5 due to the increased free volume between PMAA strata observed earlier.[40] Similarly, the stratification observed in SA-hydrated PMAA hydrogels[40] may result in different mechanical properties (Young's modulus) compared to dipped hydrogels under swollen conditions (pH > 6).

The effect of polymer molecular weight on the mechanical properties of LBL materials has mainly been studied on polyelectrolyte and hydrogen-bonded multilayers rather than hydrogels. Gao et al. demonstrated that Young's modulus rises by 50% when the M_w of PAH in (PSS/PAH) multilayer capsules is increased.[57] In contrast, Vinogradova and colleagues did not find any effect of the molecular weight of shell-forming polymers on the rigidity of (PSS/PAH) multilayer microcapsules.[58] Understanding how the sacrificial binder in ultrathin multilayer hydrogels impacts their rigidity may lead

https://doi.org/10.1021/acs.macromol.3c01253
Macromolecules XXXX, XXX, XXX−XXX

to a unique approach to controlling hydrogel properties and advancing fundamental and applied research on nanostructured hydrogels.

The exploration of nanothin hydrogel film nanomechanics holds crucial significance for expanding their utility in tissue engineering, soft robotics, and drug delivery. While various techniques have been established to modulate mechanical properties in bulk hydrogels, the precise control of mechanical response within multilayer hydrogel films remains relatively uncharted. Our prior work revealed the impact of a sacrificial binder on the dry state characteristics of multilayer hydrogels, yet the implications of hydration and resulting mechanical properties remained unresolved.[56] This study introduces an innovative strategy for regulating the mechanical behavior of multilayer hydrogel thin films through their structural organization. By regulating the molecular weight of a sacrificial polymer binder, we demonstrate the alteration of the internal architecture in multilayer hydrogels, forming distinct strata: cross-link-rich and cross-link-poor regions. This finding uncovers a novel avenue for regulating multilayer hydrogels' mechanical behavior, offering promising applications in sensing, optics, and drug delivery. Herein, we investigated how the internal organization of ultrathin PMAA multilayer hydrogels affects their rigidity. In this work, free volume in the PMAA hydrogels is controlled by (1) the molecular weight of the sacrificial binder PVPON and (2) polymer intermixing via the assembly method (dipped versus SA) employed to assemble (PMAA/PVPON) hydrogen-bonded template coatings. The hydrogen-bonded (PMAA/PVPON) templates are chemically cross-linked with ethylenediamine to obtain PMAA multilayer hydrogels. The effect of PMAA hydrogel organization on its swelling and hydration is assessed by *in situ* NR and spectroscopic ellipsometry. We have developed a constrained model to fit the NR data to determine hydrogel swelling, the number of water molecules associated with each swollen hydrogel monomer, and mass density for hydrogels synthesized using low (40,000 g mol^{-1}) and high (280,000 g mol^{-1}) M_w PVPON (40-PVPON and 280-PVPON, respectively). This parametric treatment (analogous to models of lipid hydration)[59] of the NR data enables us to explicitly translate scattering length density (refractive index) into a nanoscopic view of the association of water molecules with the hydrogel network. Colloidal probe AFM was used to assess the mechanical properties of dry and hydrated PMAA multilayer hydrogel surface coatings. The refined level of control over the internal architecture of pH-sensitive hydrogels demonstrated in this work may be advantageous for hydrogel applications in drug delivery, sensing coatings, and semipermeable materials.

EXPERIMENTAL SECTION

Materials. Poly(methacrylic acid) (PMAA, average M_w 100,000 g mol^{-1}) was acquired from Polysciences, Inc. Mono- and dibasic sodium phosphate buffers, chloroform, hydrochloric acid, and sodium hydroxide were obtained from Fisher Scientific. Poly(*N*-vinylpyrrolidone) (PVPON, nominal M_w 360 000 g mol^{-1}), sodium azide, ethylenediamine (EDA, 99%+), and branched poly(ethylenimine) (PEI, M_w 25 000 g mol^{-1}) were purchased from Alfa Aesar. Poly(styrene sulfonate) sodium salt (PSS, average M_w 70,000 g mol^{-1}) was from Sigma-Aldrich. PVPON (nominal M_w 58,000 g mol^{-1}) was purchased from Acros Organics. (3-(3-(Dimethylamino)propyl)-1-ethylcarbodiimide hydrochloride (EDC, 99%+) was from Chem-Impex International. Poly(glycidyl methacrylate) (PGMA) was synthesized from glycidyl methacrylate by radical polymerization using azobis(isobutyronitrile) in 2-butanone, as reported previously.[60] All experiments were carried out with ultrapure deionized (DI) water with a resistivity of 18.2 MΩ·cm (Evoqua). Polished 2 in.-diameter silicon wafers were purchased from University Wafer. Hydrochloric acid (0.1 M) and sodium hydroxide (0.1 M) were used to adjust the solution pH. Aqueous PVPON solutions were prepared by dissolving polymers at 10 mg mL^{-1} in DI water. PVPON solutions were then dialyzed (Spectra/Por; 20 kDa for PVPON with M_w = 58,000 g mol^{-1} and 100 kDa for 360 kDa, correspondingly) against DI water (2 L beakers) for a week. The media were replaced every 8 h. Dialyzed polymers were recovered by freeze-drying (Labconco), and their molecular weights were analyzed using gel permeation chromatography (GPC, Waters).

GPC. The molecular weights of dialyzed PVPON homopolymers and polymer dispersity ($Đ$) were determined by GPC using a solution of sodium azide (NaN_3) (200 ppm) in DI as an eluent. Measurements were performed on a Waters 1525 system equipped with a Waters 2414 refractive index detector and a Waters in-line degasser. Polymer solutions were prepared at a concentration of 5 mg mL^{-1} and separated using a set of PolySep-GFC-P 4000 (exclusion limits from 3000 to 400,000 Da) and PolySep-GFC-P 3000 (exclusion limits from 250 to 75,000 Da) columns at a flow rate of 1 mL min^{-1} at room temperature. Narrow poly(ethylene oxide) standards with molecular weights ranging from 3020 to 330,000 Da (PSS-Polymer) were used to calibrate the GPC columns. The weight-average (M_w) molecular weights were evaluated by using the Breeze 2 software package (Waters). By analyzing GPC traces of PVPON polymers (Figure S1a), the weight-average molecular weights of the polymers were found to be 40,000 g mol^{-1} ($Đ$ = 2.0), denoted as 40-PVPON and 280,000 g mol^{-1} ($Đ$ = 1.3) denoted as 280-PVPON (Figure S1a).

Assembly of Polymer Multilayer Coatings. Before polymer multilayer assembly, silicon wafers (2 cm × 5 cm) were cleaned as described elsewhere.[40] Afterward, the wafers were primed with a PGMA layer spin-coated onto the wafer surfaces from a PGMA chloroform solution (0.089 mg mL^{-1}). The wafer was then annealed at 110 °C for 1 h and rinsed with chloroform to remove unbound PGMA. An average PGMA layer had a dry thickness of 1−2 nm as measured by ellipsometry. After that, a PMAA layer was spin-coated onto the PGMA-primed wafers from a methanol solution (1 mg mL^{-1}) and annealed at 80 °C for 40 min to anchor PMAA to PGMA covalently. Unbound PMAA was then removed by rinsing the wafer with DI water. For polymer multilayer assembly at primed wafer surfaces, PMAA and PVPON polymer solutions (0.5 mg mL^{-1}, pH 2.5) prepared using phosphate buffers (0.01 M) were used to alternatingly adsorb the polymers on silicon wafer surfaces via spin-assisted (SA)[40] (Laurell Technologies spin-coater) or dipped LbL polymer assembly. For SA PVPON/PMAA multilayers, a 0.5 mg mL^{-1} PVPON solution was added in a 1.5 mL shot onto the PGMA/PMAA-primed wafers (2 cm × 5 cm) and rotated for 30 s (3000 rpm) on a spin-coater. After that, the wafer was rinsed two times with phosphate buffer solution (0.01 M, pH 2.5) for 30 s each, followed by adsorption of the PMAA layer (Figure 1) in the same manner. This surface deposition of the PVPON/PMAA bilayer was repeated until the desired number of $(PVPON/PMAA)_n$ bilayers (n) was achieved. The multilayer-coated wafers were dried under a gentle stream of nitrogen gas (Airgas). For dipped multilayers, a PGMA/PMAA-primed wafer was alternately submerged in PVPON (0.5 mg mL^{-1}, pH 2.5) and PMAA (0.5 mg mL^{-1}, pH 2.5) solutions with two rinses in phosphate buffer solution (0.01 M, pH 2.5, 30 s) between the polymer adsorption steps. This process was repeated until the desired PVPON/PMAA bilayer number was obtained, followed by wafer drying with nitrogen gas.

To obtain $(PMAA)_n$ multilayer hydrogel coatings, PMAA layers within $(PVPON/PMAA)_n$ multilayers were chemically cross-linked as described earlier.[40] Briefly, first, $(PVPON/PMAA)_n$-coated wafers were submerged into an EDC solution (5 mg mL^{-1} in 0.01 M phosphate buffer, pH 5) for 40 min to activate the carboxylic groups of PMAA, followed by rinsing with phosphate buffer (0.01 M, pH 5.0). Then, the coatings were exposed to EDA solution (0.012 mg mL^{-1}, in 0.01 M phosphate buffer, pH 5.8) for 16 h to cross-link the PMAA layers. After that, the polymer-coated wafers were rinsed with

https://doi.org/10.1021/acs.macromol.3c01253
Macromolecules XXXX, XXX, XXX−XXX

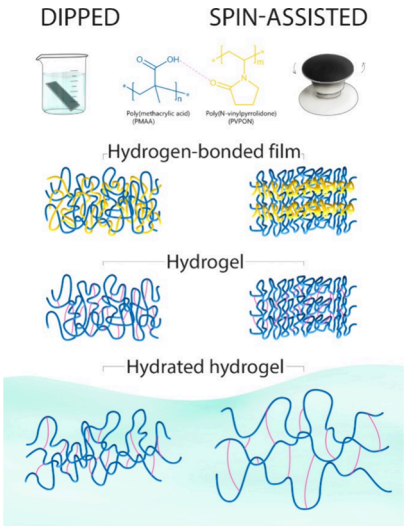

Figure 1. Using dipped (left) or spin-assisted (SA) (right) polymer multilayer assembly of PMAA and PVPON, hydrogen-bonded (PVPON/PMAA) multilayer templates were obtained. (PMAA) multilayer hydrogels were produced after cross-linking PMAA layers with EDA, followed by PVPON release at pH ≥ 8. Structured SA PMAA and intermixed dipped PMAA multilayer hydrogels swell differently in solution at pH > 5.

the 0.01 M phosphate buffer (pH 5) three times for 30 s and left in 0.01 M phosphate buffer solution at pH 8 for 48 h to swell the PMAA multilayer hydrogel and to release PVPON. The obtained PMAA multilayer hydrogel coatings on the wafers were allowed to deswell at pH 5 in 0.01 M phosphate buffer for 15 min, followed by drying at ambient conditions (Figure 1). The hydrogen-bonded (PVPON/PMAA) and (PMAA) multilayer hydrogel films obtained with PVPON of M_w 40,000 g mol^{-1} are further denoted as (40-PVPON/PMAA)$_n$ and (40-PMAA)$_n$, respectively, while those obtained using PVPON of M_w 280 000 g mol^{-1} are denoted as (280-PVPON/PMAA)$_n$ and (280-PMAA)$_n$, respectively.

Spectroscopic Ellipsometry. The thickness of surface-anchored films in the dry and wet states was analyzed with an M2000U spectroscopic ellipsometer (J.A. Woollam). Dry film measurements were obtained at 65, 70, and 75° angles of incidence between 400 and 1000 nm, and Ψ, Δ, and ellipsometric angles were fitted using a multilayer model composed of silicon, silicon oxide, and a polymer film. The thickness of SiO_2 on each wafer was determined using known optical constants. The thickness of the polymer films was determined by fitting the data using the Cauchy approximation.[61,62] The film thickness in the solution was analyzed using a 5 mL liquid flow-through cell (J.A. Woollam). Thickness measurements were obtained at a 70° angle of incidence within a cell filled with a 0.01 M phosphate buffer solution at the desired pH value. The coating thickness was determined by fitting data and adjusting the A_n, B_n, and C_n parameters until the mean squared error (MSE) for the fitted data was less than 30.

***In Situ* Attenuated Total Reflection Fourier Transform Infrared Spectroscopy (ATR-FTIR).** Chemical cross-linking of (40-PMAA)$_n$ and (280-PMAA)$_n$ hydrogels was followed by *in situ* ATR-FTIR using a Bruker VERTEX 70 FTIR spectrometer with a narrow-band mercury cadmium telluride detector. The ATR-FTIR liquid cell was constantly purged with dry nitrogen (Airgas). The ATR surface was a 50 mm × 10 mm × 2 mm rectangular trapezoidal multiple-reflection Si crystal with 45° cut beam entrance and exit surfaces (Harrick Scientific). To avoid overlap of the IR bands in the 1800−1500 cm^{-1} range with the water band, we used D_2O (99.9% isotope content, Cambridge Isotope Laboratories). The FTIR spectra were acquired at a resolution of 4 cm^{-1} with 128 averaged scans. Each spectrum was assigned a relevant background for the same ATR cell and measured using the same D_2O buffer solution. For multilayer deposition, the oxidized ATR crystal was first primed with an SA (PEI/PSS)$_{3.5}$ multilayer produced by alternating SA deposition of PEI (0.1 mg mL^{-1}, H_2O) and PSS (0.1 mg mL^{-1}, 0.01 M phosphate buffer, pH 4.5) followed by the deposition of (PMAA/PVPON)$_{10.5}$ films using either with PVPON with M_w 40,000 or 280,000 g mol^{-1}. The cross-linking of (PMAA/PVPON)$_{10.5}$ was carried out for 16 h, as described above, using EDC and EDA solutions in D_2O. PVPON release from the (PMAA)$_{10.5}$ hydrogel was performed by exposing the cross-linked (PMAA/PVPON)$_{10.5}$ coating to 0.01 M phosphate buffer in D_2O (pH 8.5) for 48 h. For cross-link density calculations, the bands of the amide and ionized carboxylic groups were determined by integrating corresponding individual deconvoluted peaks. Using OriginPro software, peak deconvolution was carried out by multiple-peak fittings to Gaussian functions.

NR. NR measurements were performed at Oak Ridge National Laboratory using the Spallation Neutron Source Liquids Reflectometer on dry samples and samples mounted in a solution cell using the data acquisition protocol described in earlier work by our group.[40] The protiated cross-linked (40-PMAA) and (280-PMAA) hydrogels were prepared on silicon wafers (2 in. in diameter, 5 mm thick) with one side polished (The Institute of Electronic Materials Technology, EL-Cat Inc.), which were exposed to 0.01 M phosphate buffer solutions (pH 5.05 and pH 6.55) prepared from D_2O. The reflectivity measurements were gathered using a series of continuous-wavelength bands (3.4 Å wide selected from 2.63 Å < λ < 16.63 Å) and incidence angles spanning across 0.6° < θ < 2.71° over a range of the wave vector transfers from 0.008 Å^{-1} < Q < 0.22 Å^{-1}, with $Q = 4\pi\sin\theta/\lambda$, where λ is the neutron wavelength and θ is the incidence angle of the neutron beam on the sample surface. By superimposing seven independently normalized angle and wavelength data sets, we created reflectivity curves over the whole Q range. By altering the incident-beam apertures, the relative instrumental resolution ($\delta Q/Q$ = 0.023) and the sample footprint were kept constant. SA deposition of PVPON and PMAA onto PGMA/PMAA-primed wafers was used to assemble 20-bilayer (PVPON/PMAA) films as described above, except that 3 mL solution shots were used, followed by cross-linking and PVPON release, as described above. The dry thickness measurements were performed in air, and the *in situ* measurements were performed using a sample cell with a clean, 10 mm-thick Si wafer and a dry sample wafer separated by an O-ring (1 mm thick). The 3 mL compartment enclosed by the two Si wafers and the O-ring was filled and emptied with buffer solution via channels that were bored through the clean Si wafer. Measurements were performed with the film compressed between two aluminum plates at room temperature (~25 °C) by using a neutron beam incident from within the sample substrate. A 10 mL plastic syringe was used to inject 0.01 M phosphate buffer solution into the flow-through cell to study pH-dependent (PMAA)$_{20}$ hydrogel swelling. The cell was filled with a buffer solution for 2 min, and then the solution was exchanged with a fresh buffer solution and allowed to equilibrate for 15 min. *In situ* NR measurements were collected from samples exposed to 0.01 M phosphate buffer solutions with pH values of 5.05 and 6.55. When the pH was changed, the solution volume was flushed three times before measurement.

Constrained Model of NR Data. A complete description of the construction of the constrained model is provided in the Supporting Information. Knowledge of film stoichiometry enabled the application of a more sophisticated layer hydration model, wherein the film's depth-dependent swelling is parametrized in terms of the number of water molecules per monomer formula unit. Briefly, the known stoichiometry of the dry network and its molar volume measured by NR can be used to infer the number of associated water molecules in the buffer-swollen hydrogel via a subsequent NR measurement (see the Supporting Information for details). The final fitted parameters for the six data sets used in this work are contained in Tables S1−S15 in the Supporting Information. The model fit to specular reflectivity is sensitive to the layer thickness (d), scattering length density (Σ), and interfacial interdiffusion or roughness (σ). According to the fitting model, the error function interface is produced by the full width at half-maximum (fwhm) of a Gaussian convolved with a step function.

https://doi.org/10.1021/acs.macromol.3c01253
Macromolecules XXXX, XXX, XXX−XXX

The quality of the fit was assessed by minimizing χ^2 while keeping the thickness and refractive index within the realm of appropriate values, consistent with ellipsometry data.

Atomic Force Microscopy (AFM). High-resolution topography images of (40-PMAA) and (280-PMAA) multilayer hydrogels were collected using an atomic force microscope (NTEGRA AFM; NT-MDT Spectrum Instruments) equipped with an SPM system controller. NSG30, NSG03, and colloidal NSG01 Bio 300/Au probes were acquired from NT-MDT Spectrum Instruments. Roughness and mechanical property measurements in the hydrogel dry state were carried out using a pyramidal sharp NSG30 probe (tip curvature radius <10 nm, force constant 22−100 N m^{-1}) over 1 μm^2 areas at different locations of 10 μm^2 images at a constant scan rate of 1 Hz. A pyramidal sharp NSG03 probe (tip curvature radius = 10 nm, force constant 0.35−6.1 N m^{-1}) was used to collect hydrogel roughness images under liquid, and high-resolution topography images were collected over 2 μm^2 areas at different locations of 10 μm^2 images at a constant scan rate of 0.8 Hz. The surface roughness was calculated as the root-mean-square (rms) average from the obtained images. A colloidal NSG01 Bio 300/Au probe (sphere curvature diameter = 300 nm, force constant 1.45−15.1 N m^{-1}) was utilized to prevent sharp-tip infiltration into the soft hydrogel during mechanical property measurements under liquid for scanning over 1 μm^2 areas at different locations of 10 μm^2 images at a constant scan rate of 1 Hz. The hydrogel samples were synthesized with dry thicknesses of more than 80 nm to avoid any effect from the silicon wafer during AFM indentation measurements as the deformation of the sample did not exceed 10% of the film thickness. For elasticity measurements, the approach curve was fitted by the Hertz model for a 300 nm radius colloidal probe possessing minimal adhesion to assess modulus in fully elastic, low-adhesion, and uniform films, aligning with prior observations in PMAA multilayer hydrogel films with low adhesion.[19] The Hertz model extension, Derjaguin−Muller−Toporov (DMT) model,[63] was used to extract the elastic modulus of polymer films at small indentation depths using a built-in software. A surface scratch method was used to assess the hydrogel thickness, which involved cutting a vertical scratch through a dry film using a razor. Topographical images (30 μm^2) across the cut area were acquired in tapping mode. The height difference between the bare wafer region and the hydrogel surface was used to compute the film thickness.

RESULTS AND DISCUSSION

Synthesis of PMAA Multilayer Hydrogels with a Sacrificial Binder of Varied Molecular Weight. We synthesized hydrogen-bonded multilayer (PVPON/PMAA) templates through dipped or SA LbL assembly using sacrificial layers of PVPON with molecular weights of 40,000 or 280,000 g mol^{-1}, denoted as 40-PVPON and 280-PVPON, respectively, and PMAA (M_w 100,000 g mol^{-1}) (Figure 1). Spectroscopic ellipsometry confirmed the linear growth of both thin, 10-bilayer, and thick, 40-bilayer SA (40-PVPON/PMAA)$_n$ and (280-PVPON/PMAA)$_n$ multilayers (Figure S1b,c).

The overall hydrogen-bonded multilayer thickness, measured by ellipsometry, increased from 120 ± 2 to 143 ± 3 nm for a 40-bilayer (PVPON/PMAA) multilayer when the molecular weight of PVPON was increased from 40,000 to 280,000 g mol^{-1} (Figure S1c), which agrees with our previous findings and literature reports.[39,56] The average bilayer thicknesses were 3.2 ± 0.2 and 3.7 ± 0.2 nm for (40-PVPON/PMAA) and (280-PVPON/PMAA) multilayers, respectively. The individual thickness of the PMAA layer within the (40-PVPON/PMAA) multilayers was slightly smaller than that in the (280-PVPON/PMAA) films and was 2.5 ± 0.3 and 2.6 ± 0.3 nm, respectively. Based on the individual layer thickness data, 40-PVPON comprised 22% by film thickness while 280-PVPON comprised 30%, which agrees with our previous finding for PVPON with M_w = 55,000 g mol^{-1} that adsorbed at 28% by thickness in the (PVPON/PMAA) hydrogen-bonded multilayer assembled at pH = 2.5.[56] The observed bilayer thickness increase when 280-PVPON was used instead of 40-PVPON is also consistent with the increasing radius of gyration of PVPON, R_g, in solution. Given the PVPON persistence length of 1 nm,[64] the estimated R_g values for 40-PVPON and 280-PVPON are 3.9 and 10.3 nm, respectively. The corresponding diameters of gyration ($2R_g$) for 40-PVPON and 280-PVPON chains in solution are much larger than the individual PVPON thicknesses in hydrogen-bonded (40-PVPON/PMAA) and (280-PVPON/PMAA) films, indicating that surface adsorption of 40-PVPON and 280-PVPON leads to the PVPON chain flattening, a common feature in SA polymer deposition at surfaces.[55,56] The average individual thicknesses of PVPON layers are 0.7 and 1.1 nm for 40-PVPON and 280-PVPON, respectively, similar to monolayer-like films, which can be due to strong hydrogen bonding between PMAA and PVPON and spinning during SA assembly.

The corresponding (40-PMAA) and (280-PMAA) multilayer hydrogels were synthesized (Figure 1) upon chemical cross-linking of (40-PMAA/PVPON) and (280-PMAA/PVPON) hydrogen-bonded multilayers with EDA and the subsequent release of PVPON templating chains at pH ≥ 8. The thicknesses of cross-linked (40-PMAA) and (280-PMAA) multilayer hydrogel films demonstrated a linear dependence on PMAA layer number, with average PMAA layer thicknesses of 2.1 ± 0.2 and 2.6 ± 0.3 nm for (40-PMAA) and (280-PMAA) hydrogels, respectively, as measured by ellipsometry for 10-, 20-, 30-, and 40-layer networks (Figure 2a). These results on PMAA layer thickness correlate well with the individual PMAA thicknesses obtained for (PVPON/PMAA) hydrogen-bonded templates, as discussed above.

ATR-FTIR analysis confirmed the synthesis of a PMAA hydrogel from a (PVPON/PMAA)$_{10.5}$ surface-anchored multi-

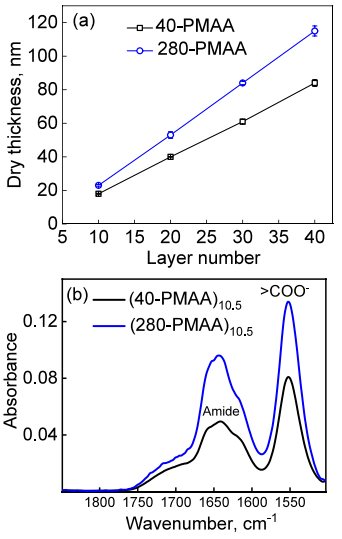

Figure 2. (a) Thickness of dry SA (40-PMAA) and (280-PMAA) films measured by spectroscopic ellipsometry. 40-PMAA and 280-PMAA stand for PMAA hydrogels prepared from PVPON with molecular weights of 40,000 or 280,000 g mol^{-1}, respectively. (b) *In situ* FTIR spectra of SA (40-PMAA)$_{10.5}$ and (280-PMAA)$_{10.5}$ hydrogels at pH 9. Absorbance peaks at 1641 and 1551 cm^{-1} correspond to amide and ionized carboxylic groups (>COO$^-$), respectively.

https://doi.org/10.1021/acs.macromol.3c01253
Macromolecules XXXX, XXX, XXX−XXX

layer and PVPON release at basic pH. ATR-FTIR serves as a widely utilized technique for assessing functionality and cross-linking of nanothin planar films, as previously demonstrated.[65] ATR-FTIR's high sensitivity facilitates precise analysis of functional group incorporation within the hydrogel network. Before PMAA cross-linking, the FTIR spectrum of the $(PVPON/PMAA)_{10.5}$ hydrogen-bonded multilayer displays the carbonyl stretching vibration bands of protonated carboxylic groups (−COOH) at 1700 cm^{-1} and the carbonyl groups (−C═O) in the pyrrolidone ring at 1647 cm^{-1} (Figure S2, line 1). Upon activation of PMAA carboxylic groups with EDC, new absorbance bands appear at 1755 and 1801 cm^{-1} due to the stretch vibrations of C═O in the PMAA ester while PVPON's presence within the multilayer is observed by the butyrolactam carbonyl at 1647 cm^{-1} (Figure S2, line 2).

ATR-FTIR analysis of the cross-linked coating at pH 9 confirmed PMAA cross-linking as an amide I absorbance band appears in the 1600−1700 cm^{-1} region (Figure S2, line 3), while the carboxylate vibrational band is present at 1550 cm^{-1}. FTIR spectra of PMAA hydrogels obtained from $(40\text{-}PVPON/PMAA)_{10.5}$ and $(280\text{-}PVPON/PMAA)_{10.5}$ films also show higher absorbances for both amide I and COO^- bands of the $(280\text{-}PMAA)_{10.5}$ hydrogel film compared to those of the $(40\text{-}PMAA)_{10.5}$ film (Figure 2b), which confirms the larger thickness of (280-PMAA) surface hydrogels as measured by ellipsometry (Figure 2a).

Analysis of the deconvoluted amide I band[66] containing its fine vibrational components of C═N at 1700 cm^{-1}, C═O at 1670 cm^{-1}, and C−N at 1625 cm^{-1} and the carboxylate band for $(40\text{-}PMAA)_{10.5}$ and $(280\text{-}PMAA)_{10.5}$ surface-anchored hydrogels revealed similar ratios of integrated peak absorbances of total amide to the amide and carboxylate of 0.50 and 0.52, respectively (Figure S3). These data imply that the cross-link densities of the two PMAA hydrogel films are similar under the same cross-linking conditions and hydrogel swelling can be used to explore the effect of the network's free space on PMAA hydrogel mechanical properties.

Effect of Sacrificial PVPON Molecular Weight on PMAA Multilayer Hydrogel Hydration. We explored the effect of a sacrificial PVPON molecular weight on the hydration of resultant PMAA hydrogels. Hydration of PMAA multilayer hydrogels at pH 5 leads to increased hydrogel thickness, which increases for both pH > 5 and pH < 5 due to ionization of carboxylic groups (pH > 5 as PMAA $pK_a \sim 5.9$)[67] or primary amine groups (pH < 5) after EDA cross-linking.[67] The PMAA hydrophilicity has been shown to result in the retention of large amounts of water inside PMAA multilayer hydrogels.[68] We analyzed the swelling of the SA PMAA hydrogels due to the ionization of PMAA carboxylic groups at pH > 5 using *in situ* ellipsometry.

The SA 280-PMAA multilayer hydrogels consistently showed about 30% greater swelling at pH 6.5 compared with that of 40-PMAA hydrogels (Figure 3). For example, the average hydrogel swelling ratios, calculated as the ratio of the hydrogel thickness at pH = 6.5 to its dry thickness, were 6.43 ± 0.06, 6.13 ± 0.18, 5.98 ± 0.04, and 6.15 ± 0.07 for 10-, 20-, 30-, and 40-layer (280-PMAA) hydrogels, compared with 4.6 ± 0.1, 4.24 ± 0.06, 4.23 ± 0.09, and 4.18 ± 0.01 for 10-, 20-, 30-, and 40-layer hydrogels of 40-PMAA (Figure 3). It is worth noting that for the thinnest hydrogels (10-layer PMAA) for both 40-PMAA and 280-PMAA, the swelling ratios are slightly but consistently higher than the ratios for thicker hydrogels (>10 PMAA layers) (Figure 3). This swelling behavior was

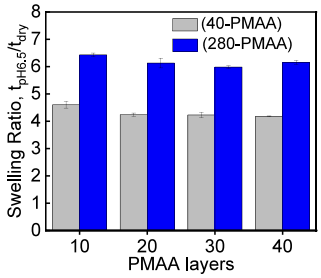

Figure 3. Swelling ratios of SA 40-PMAA and 280-PMAA multilayer hydrogels of different thicknesses calculated as the ratio of hydrogel thickness at pH 6.5 ($t_{pH6.5}$) to the dry hydrogel film thickness (t_{dry}). Hydrogel thickness was measured by using *in situ* ellipsometry.

previously demonstrated for surface-attached nanothin hydrogels made from copolymers of methacryloyloxybenzophenone and dimethylacrylamide where a higher mixing osmotic pressure experienced by thinner hydrogels could be partially relieved by a more significant expansion in one direction resulting in a higher linear swelling ratio.[69] Similarly, a higher swelling ratio (SR = 3.2) for thinner coatings (40 nm) was observed for surface-attached poly(*N*-isopropylacrylamide) hydrogels, compared with SR = 1.6 for thicker 100 nm hydrogels.[70]

Given the similar cross-link densities for 40-PMAA and 280-PMAA hydrogels confirmed by ATR-FTIR analysis (Figure S3), the ellipsometry data on hydrogel swelling at pH 6.5 suggests that the PMAA hydrogels obtained with PVPON of a higher molecular weight should exhibit greater hydration than those synthesized with lower-M_w PVPON. We employed neutron reflectivity (NR) to quantify the hydrogel hydration for both types of PMAA hydrogel coatings in phosphate buffer solutions.

The dependence of the refractive properties of neutron waves on isotopic composition, particularly the strong contrast between protium (^1H) and deuterium (^2H), and control of stoichiometry enable us to deduce nanoscopic structure from scattering length density (refractive index), a continuum quantity. Figure 4 shows NR data (Figure 4a,c,e) and related scattering length density (SLD) profiles (Figure 4b,d,f) for 20-bilayer 40-PMAA and 280-PMAA multilayer hydrogels in dry (Figure 4a,b) and hydrated states at pH 5.05 (Figure 4c,d) and pH 6.55 (Figure 4e,f). Normalized NR RQ^4 is plotted versus wave vector transfer Q ($Q = 4\pi\sin\theta/\lambda$, where λ is the neutron wavelength and θ is the incident angle) (Figure 4a,c,e). Physical and scattering parameters for NR fitting curves are summarized in the Supporting Information (Tables S1−S15). Initial hydrogel thickness was determined using ellipsometry measurements and then modified to fit the NR data using a constrained model of the NR data (see the Supporting Information). The density distribution in the direction normal to the film surface is presented in the SLD profiles derived from fitting the NR data (Figure 4b,d,f).

For dry $(40\text{-}PMAA)_{20}$ and $(280\text{-}PMAA)_{20}$ hydrogels, the corresponding SLD profiles do not resolve individual PMAA layers within the hydrogel. The PMAA hydrogel is observed between the silicon-PGMA interface and the polymer−air interface (Figure 4a,b). The total thicknesses of $(40\text{-}PMAA)_{20}$ and $(280\text{-}PMAA)_{20}$ hydrogel films in the dry state were measured to be 46.7 ± 0.1 and 60.8 ± 0.1 nm, respectively (Table 1). The 30%-thickness difference between the two hydrogels obtained in NR analysis agrees with the 33% larger

https://doi.org/10.1021/acs.macromol.3c01253
Macromolecules XXXX, XXX, XXX−XXX

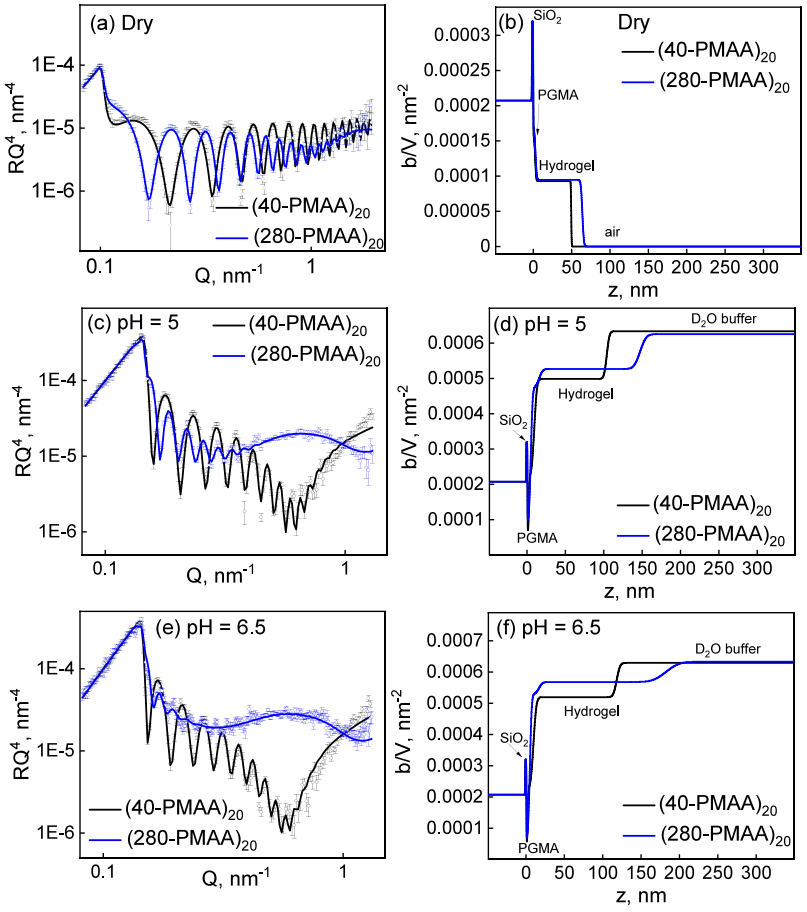

Figure 4. Normalized NR data (a, c, e) and corresponding SLD profiles (b, d, f) of SA 20-layer (40-PMAA) and (280-PMAA) hydrogel films in the dry (a, b) and hydrated at pH = 5.05 (c, d) and 6.55 (e, f) states.

Table 1. Thickness (d), the Number of D_2O Molecules Associated with Each Monomer in the Swollen Hydrogel (n_w), the Number of D_2O Molecules per Unit of Volume (N_w), Swelling Ratio (SR), and Density (ρ) of $(40\text{-PMAA})_{20}$ and $(280\text{-PMAA})_{20}$ Hydrogels Obtained from NR Data

sample	state	d (nm)	n_w	N_w(nm^{-3})	SR	ρ (g cm^{-3})
$(40\text{-PMAA})_{20}$	dry	46.7 ± 0.1				0.95 ± 0.01
	pH 5.05	101.2 ± 0.1	8.2 ± 0.1	23.5 ± 0.3	2.17 ± 0.01	1.20 ± 0.01
	pH 6.55	115.1 ± 0.2	9.8 ± 0.1	25.0 ± 0.4	2.46 ± 0.01	1.20 ± 0.01
$(280\text{-PMAA})_{20}$	dry	60.8 ± 0.1				0.93 ± 0.01
	pH 5.05	143.5 ± 0.6	9.6 ± 0.2	25.3 ± 0.5	2.36 ± 0.01	1.23 ± 0.02
	pH 6.55	171.3 ± 1.7	12.2 ± 0.2	27.2 ± 0.6	2.82 ± 0.03	1.23 ± 0.02
D2O				33.4		1.110

thickness of the 20-layer (280-PMAA) hydrogel film compared to that of (40-PMAA) with the dry thicknesses of 53 and 40 nm, respectively, measured by ellipsometry (Figure 2a). The slightly larger thicknesses of the dry hydrogel film measured by NR compared to those found by ellipsometry were observed earlier for multilayer hydrogel stacks of PVPON and poly(*N*-vinylcaprolactam) and were attributed to varied ambient humidity between the experiments affecting the baseline thicknesses of the coatings.[71] Conversely, the observed differences in NR and ellipsometry thickness measurements may be due to a higher density of (280-PMAA) hydrogel compared to the (40-PMAA) film since ellipsometry measures the product of refractive index and thickness.

Upon exposure to phosphate buffer solutions (in D_2O) at pH = 5.05 and 6.55, both hydrogels expanded due to hydration and ionization of PMAA carboxylic acid groups (Figure 4d,f). The lowest SLD at the silicon interface is due to a nonswollen hydrophobic layer of PGMA, followed by the swollen PMAA hydrogel. The SLD region with the highest scattering density is due to the D_2O buffer solution.

The $(40\text{-PMAA})_{20}$ hydrogel swelling ratio, SR, calculated from the NR data at pH 5.05 as the ratio of hydrated to dry cross-linked polymer thickness was found to be 2.17, while the SR for $(280\text{-PMAA})_{20}$ at pH 5.05 was 2.36 (Table 1). Similarly, a more extensive swelling of $(280\text{-PMAA})_{20}$ at pH 6.55 was observed compared to the $(40\text{-PMAA})_{20}$ hydrogel with corresponding SRs of 2.82 ± 0.03 and 2.36 ± 0.01, respectively (Table 1).

The greater hydration of the $(280\text{-PMAA})_{20}$ hydrogel was also confirmed by comparing the number of water (D_2O) molecules associated with each monomer in the swollen hydrogel (n_w) (Table 1) obtained from fitting the NR data (see

https://doi.org/10.1021/acs.macromol.3c01253
Macromolecules XXXX, XXX, XXX−XXX

the Supporting Information). Thus, at pH 5.05, n_w values of 8.2 ± 0.1 and 9.6 ± 0.2 were found for $(40\text{-PMAA})_{20}$ and $(280\text{-PMAA})_{20}$, respectively (Table 1) with a similar trend at pH 6.55 with the n_w values increasing to 9.8 ± 0.1 and 12.2 ± 0.2 for $(40\text{-PMAA})_{20}$ and $(280\text{-PMAA})_{20}$, respectively (Table 1). Hydration characterized by the number of D_2O molecules per volume (N_w) follows the same trend and increases from 23.5 ± 0.3 D_2O molecules per nm^3 at pH 5.05 to 25.0 ± 0.4 at pH 6.55 for $(40\text{-PMAA})_{20}$. The volume density of D_2O was larger for $(280\text{-PMAA})_{20}$ at pH 5.05 (N_w = 25.3 ± 0.5) and increased to 27.2 ± 0.6 D_2O molecules per nm^3 at pH 6.55 (Table 1). Note that the mass density (ρ, g cm^{-3}) of the $(40\text{-PMAA})_{20}$ hydrated film was slightly less than that of the $(280\text{-PMAA})_{20}$ hydrogel at both studied pH values and explains our ellipsometry data showing a slightly larger thickness of the (280-PMAA) coatings.

Since the average cross-link densities for the two PMAA hydrogels were found to be similar, as discussed above, polymer chain conformation and the distribution of hydrogel's free space must affect the hydration of the PMAA hydrogels.[72] For instance, Selin et al. studied the effect of polymer−polymer interactions on the swelling properties of poly[(trifluoroethoxy)(carboxylatophenoxy)phosphazene] (FP60)/branched polyethylenimine (BPEI) and poly[di(carboxylatophenoxy)phosphazene] (PCPP)/(BPEI) multilayers.[73] They showed that weakly bound PCPP/BPEI multilayers exhibited a 45% water uptake, while the strongly bound FP60/BPEI multilayer films showed only 10% uptake.[73] Such a dramatic difference in water uptake was explained by the differing numbers of monomer units participating in polymer−polymer interactions in the two systems. Since weakly bound multilayers feature a lower density of interacting polymer−polymer pairs, there is a greater density of unbound monomer units available for water uptake.[36,73] Conversely, strongly interacting polyelectrolytes have most of their binding sites involved in polymer−polymer interactions, resulting in lower water uptake.[36,73] The same trend was observed by Sukhishvili and colleagues when studying the effect of polymer deposition time on the internal structure and multilayer properties of PMAA/quaternized poly-2-(dimethylamino)ethyl methacrylate (QPC) multilayer films.[42] They showed that enhanced loop formation by QPC resulted in higher water uptake.[42] In this study, more PMAA deposited in the 280-PVPON-templated films may result in more chain loops in the 280-PMAA hydrogel, leading to enhanced hydration compared to 40-PMAA.

During hydration, void areas were filled with water. Due to electrostatic repulsion between ionized carboxylic groups, polymer chains expand within the hydrogel network as solution pH increases and freely bound water is absorbed. Matyjaszewski and colleagues showed that the amount of bulk water contained within a poly(2-(2-methoxyethoxy)ethyl methacrylate) hydrogel is determined by network topology and is related to the expansibility of the network.[74] The greater R_g of 280-PVPON results in 30% thicker PVPON layers between the PMAA layers in the template films, decreasing the volume density of PMAA within the intermixed nominal PVPON layers. Upon cross-linking, this lower density of available PMAA results in a more open network and more space for PMAA chain expansion at high pH after the PVPON is released. This more open network leads to greater hydration of 280-PMAA relative to 40-PMAA hydrogels.

Mechanical Properties of SA (40-PMAA) and (280-PMAA) Hydrogels. AFM imaging of $(40\text{-PVPON-PMAA})_{40}$ and $(280\text{-PVPON-PMAA})_{40}$ hydrogen-bonded multilayer templates and their corresponding $(40\text{-PMAA})_{40}$ and $(280\text{-PMAA})_{40}$ multilayer hydrogel films in the dry state revealed a 30% increase in surface roughness of the coatings for the larger molecular weight PVPON (Figures S4a,b and S5). The rms surface roughness was measured to be 0.57 ± 0.03 nm for $(40\text{-PVPON/PMAA})_{40}$ and 0.80 ± 0.03 nm for $(280\text{-PVPON/PMAA})_{40}$ multilayers, which agrees with typical rms values of ∼1−3 nm reported for SA multilayer films.[39,40] This surface roughness trend persisted for the corresponding dry multilayer hydrogel films, which exhibited rms values of 0.57 ± 0.05 nm for $(40\text{-PMAA})_{40}$ and 0.89 ± 0.04 nm for $(280\text{-PMAA})_{40}$ hydrogels (Figures S4c,d and S5). A surface roughness increase upon increasing polymer molecular weight has been reported for dipped and SA multilayer coatings and was attributed to more loopy chain conformations for polymers with higher M_w.[39,40] For instance, an increase in M_w of hyaluronic acid (HA) from 6.4 to 1500 kDa resulted in a fourfold roughness increase for dipped (HA/poly(L-lysine)) multilayer films.[75] A comparison between SA and dipped hydrogen-bonded assemblies of silk fibroin/poly(*N*-vinylcaprolactam) (PVCL) revealed a 1.5-fold increase in the film surface roughness when PVCL M_w was increased from 5 to 80 kDa.[39]

In this study, the hydration of $(PMAA)_{40}$ hydrogels was accompanied by increased surface roughness (Figure S4e−h). For instance, the rms surface roughness of the $(40\text{-PMAA})_{40}$ hydrogel increased by a factor of 3.9 (rms = 2.2 ± 0.2 nm) when the hydrogel was exposed to pH 5 buffer solution and by a factor of 5.1 at pH 6.5 (rms = 2.9 ± 0.3 nm (Figure S5). Similarly, the surface roughness of the $(280\text{-PMAA})_{40}$ hydrogel increased to 3.7 ± 0.3 nm at pH 5 and 4.3 ± 0.3 nm at pH 6.5, with a 30% larger roughness observed for the larger molecular weight PVPON-templated hydrogel. The hydrogel films did not show surface wrinkling (buckling instabilities) after swelling/drying. Hayward and colleagues demonstrated earlier that the dry thickness for the buckling onset for homopolymer and block copolymer films was more than 130 nm at 6%-cross-linking degrees. No buckling was reported for thinner hydrogel films at the same cross-link densities. The minimum thickness for buckling instability onset was also reported to increase with higher cross-linking for the films anchored to silicon surfaces.[76] Our study used hydrogel films with dry thicknesses up to 125 nm and high cross-linking degrees. AFM imaging data of the surface-anchored hydrogel films after swelling and drying confirmed the absence of surface wrinkling after film hydration and drying (Figure S6). This observation agrees with our previous reports on the uniform surface morphology of $(PVPON)_n(poly(N\text{-vinylcaprolactam})_m$ double-strata multilayer hydrogels that also did not exhibit surface wrinkling.[71]

The effect of increased roughness upon film hydration has previously been reported for both hydrogen-bonded and ionically paired polyelectrolyte multilayers and explained by polymer chain relaxation through chain untangling and loop extension during network hydration.[40,77,78] For example, a swelling-induced increase in roughness from 16 nm in the dry state to 106 nm in solution was reported for ionically paired PSS/poly(diallyldimethylammonium chloride) multilayer coatings.[77]

The mechanical properties of the PMAA multilayer hydrogel films in dry and hydrated states were evaluated by using AFM nanoindentation. The AFM nanoindentation technique has

https://doi.org/10.1021/acs.macromol.3c01253
Macromolecules XXXX, XXX, XXX−XXX

been proven suitable for soft multilayer films with rigidities in the range of GPa to kPa.[48,65,79] Young's modulus of soft, hydrated films was determined by indentation using the colloidal probe. For elasticity measurements, the approach curve was fitted by the Hertz model for a 300 nm-radius colloidal probe possessing minimal adhesion to assess moduli in fully elastic, nonadhesive, and uniform films, aligning with prior observations in PMAA multilayer hydrogel films with low adhesion.[19] The Hertz model extension, the DMT model, was used to extract the elastic modulus of polymer films at small indentation depths.[80] Young's modulus maps were collected over 1 μm^2 areas of the hydrogels using a colloidal probe (Figure 5). The Young's modulus of the dry hydrogel films was

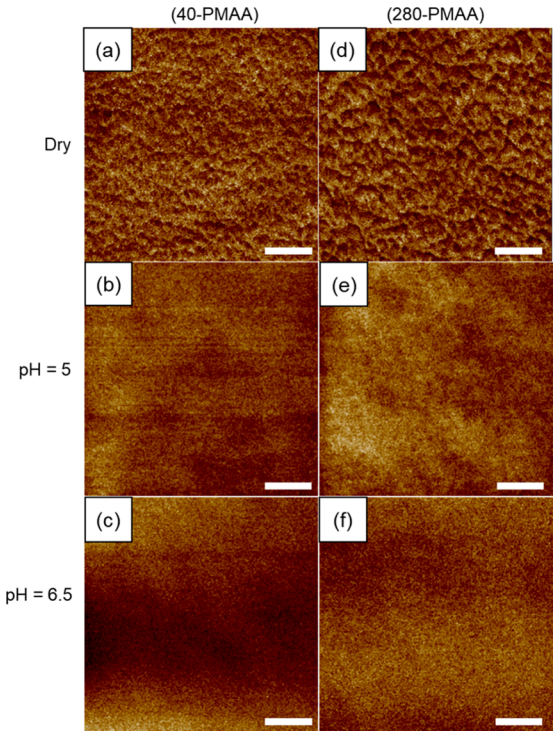

Figure 5. Young's modulus maps of SA $(40\text{-PMAA})_{40}$ (a–c) and $(280\text{-PMAA})_{40}$ (d–f) hydrogel films at the dry state (a,d), pH 5 (b,e), and pH 6.5 (c,f) collected by AFM nanoindentation. The scale bar is 200 nm.

found to be homogeneous over the analyzed areas (Figure 5a,d) and was similar for both $(40\text{-PMAA})_{40}$ and $(280\text{-PMAA})_{40}$ hydrogels with elasticity values of 2.0 ± 0.2 and 2.0 ± 0.1 GPa, respectively (Table 2). These results are consistent with earlier findings for polyelectrolyte multilayer films in the dry state, where Young's modulus was typically measured within a range of a few gigapascals depending on preparation technique and film composition.[78,81] The Young's modulus of both $(PMAA)_{40}$ dry hydrogel films found in this work agrees with the elasticity modulus of 1.9 GPa reported for $(PMAA)_{60}$ dry hydrogel films in an earlier study.[78]

Upon hydration, $(40\text{-PMAA})_{40}$ and $(280\text{-PMAA})_{40}$ hydrogels exhibited a several-order-of-magnitude homogeneous decrease in the elastic modulus over 1 μm^2 analyzed surface areas (Figure 5b,c,e,f). Specifically, Young's modulus of the $(40\text{-PMAA})_{40}$ hydrogel was found to be 43 ± 6 MPa when submerged in the pH 5 solution, drastically decreasing to 6 ± 0.4 MPa in solution at pH 6.5 (Table 2, Figure 6). Water is

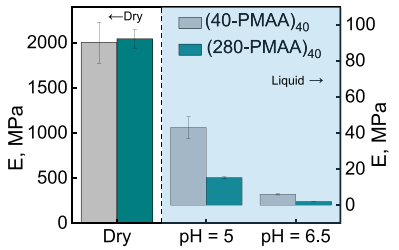

Figure 6. Young's modulus of SA $(40\text{-PMAA})_{40}$ and $(280\text{-PMAA})_{40}$ multilayer hydrogels measured via AFM nanoindentation in both dry (left scale) and hydrated (right scale) conditions at pH 5 and 6.5 (0.01 M phosphate buffer; equilibrated for 20 min).

known as a plasticizer for hydrogels, leading to significant softening due to enhanced chain mobility in swollen multilayer coatings.[82] Nolte et al. reported a 10-fold reduction in Young's modulus for ionically paired PAH/PSS multilayers after immersion in water.[82] We previously observed a 25-fold Young's modulus decrease for a $(PMAA)_{60}$ multilayer hydrogel at pH 5, followed by a 136-fold reduction in elastic modulus at pH 6.5 compared to the dry state.[78]

Remarkably, upon swelling in solution at pH 5, a $(280\text{-PMAA})_{40}$ hydrogel was softer than its $(40\text{-PMAA})_{40}$ counterpart, featuring an approximately three-times lower Young's modulus of 15 ± 1 MPa in solution at pH 5 (Table 2, Figure 6). A similar difference in Young's modulus between $(40\text{-PMAA})_{40}$ and $(280\text{-PMAA})_{40}$ was observed in solution at pH 6.5, where the $(280\text{-PMAA})_{40}$ hydrogels had an elasticity of 2 ± 0.1 MPa compared to 6 ± 0.1 MPa for $(40\text{-PMAA})_{40}$ (Table 2, Figure 6). Therefore, despite both hydrogels having similar thicknesses in the dry state (Table 2) and similar cross-link densities, the $(280\text{-PMAA})_{40}$ hydrogel demonstrated greater swelling both at pH 5 and pH 6.5 (Figure 4, Table 2) and higher hydration (Table 1), resulting in lower rigidity of the SA 280-PMAA hydrogel compared to the SA 40-PMAA hydrogel (Table 2, Figure 6).

This behavior can be explained by considering the variable density of cross-links throughout the PMAA hydrogel. Earlier, we demonstrated that the SA PMAA multilayer hydrogel could be viewed as a network of alternating cross-link-rich and cross-link-poor strata.[40] The cross-link-rich strata coincide with precursor PMAA layers before cross-linking. In contrast, the

Table 2. Thickness and Average Young's Modulus of 40-Bilayer SA 40-PMAA and 280-PMAA Surface Multilayer Hydrogel Films in the Dry State and in Solutions at pH 5 and pH 6.5[a]

	thickness (nm)			Young's modulus		
	dry	pH 5	pH 6.5	dry (GPa)	pH 5 (MPa)	pH 6.5 (MPa)
(40-PMAA)	96 ± 2	266 ± 2	400 ± 2	2.0 ± 0.2	43 ± 6	6.0 ± 0.4
(280-PMAA)	116 ± 4	367 ± 5	668 ± 3	2.0 ± 0.1	15 ± 1	1.9 ± 0.1

[a]The hydrogel thickness was measured by ellipsometry, and Young's modulus was analyzed over 1 μm^2 areas using AFM nanoindentation.

https://doi.org/10.1021/acs.macromol.3c01253
Macromolecules XXXX, XXX, XXX–XXX

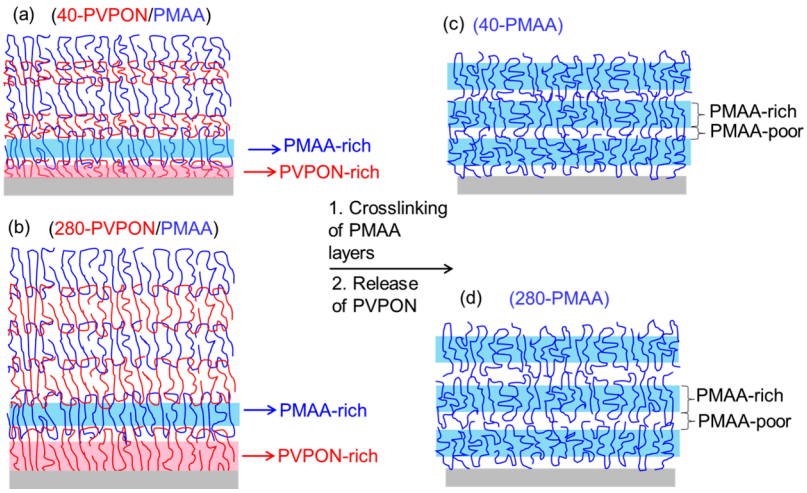

Figure 7. Initial (PVPON/PMAA) hydrogen-bonded multilayer films assembled via spin-assisted LbL using a (a) 40 kDa PVPON or (b) 280 kDa PVPON sacrificial binder with alternating layers of PVPON (PVPON-rich) and PMAA (PMAA-rich) with intermixing between the layers. After cross-linking the PMAA and release of PVPON from the network, the corresponding PMAA multilayer hydrogels (c, d) are obtained that consist of PMAA-rich and PMAA-poor strata.

cross-link-poor strata are centered between the adjacent PMAA layers in the cross-linked hydrogel in spaces where PVPON layers were located in the precursor (PMAA/PVPON) film.

Our earlier NR study revealed a higher density of cross-links in precursor PMAA-rich strata and a lower density in precursor PVPON strata.[40] This difference in cross-link distribution between cross-link-rich and cross-link-poor strata was explained by the greater availability of cross-linking partners in the PMAA layers relative to the PVPON layers. As a result, the cross-link-rich strata were shown to swell less than the cross-link-poor strata in the SA PMAA multilayer hydrogel.[40] Given the similar average cross-link density in SA 40-PMAA and 280-PMAA hydrogels, thinner PVPON layers between the PMAA adjacent layers in the precursor 40-PVPON/PMAA films lead to greater intermixing across PVPON layers between adjacent PMAA layers. The resulting 40-PMAA hydrogel features a greater density of cross-links in the cross-link-poor (former PVPON) space compared to the 280-PMAA hydrogel. Our current NR hydration and swelling ratio data (Table 1) are consistent with these earlier findings for swollen PMAA multilayer hydrogels obtained from PVPON with M_w = 55,000 Da.[40] Similarly, stiffer and more compact hydrogels were demonstrated in a different study when the free volume was decreased in methacrylated gelatin and alginate-based hydrogels.[29]

Our ellipsometry and NR results imply that controlling the density of cross-links between PMAA-adjacent layers in PMAA multilayer hydrogels by changing the molecular weight of templating PVPON can lead to a different total swelling of the hydrogel. Thus, unlike controlling bulk hydrogel cross-link density,[19,78] our approach enables the imposition of a nanostructured organization on the hydrogel and a selective modulation of the cross-link density within the PMAA hydrogel strata. Figure 7 schematically shows PMAA multilayer hydrogels obtained from initial SA (PVPON/PMAA) hydrogen-bonded template coatings (Figure 7a,b) via cross-linking PMAA followed by the release of PVPON from the PMAA network. The resulting PMAA multilayer hydrogels consist of alternating stacks of PMAA-rich and PMAA-poor strata (Figure 7c,d). Our FTIR analysis confirmed that the two hydrogels had similar average cross-link densities. However, as discussed above, the density of cross-links within PMAA-rich strata is greater than that in PMAA-poor strata, as we demonstrated earlier for PMAA hydrogels obtained using M_w 55 kDa PVPON.[40]

Overall, consistently greater swelling ratios and network hydration for the 280-PMAA multilayer hydrogel suggest greater intermixing of PMAA-adjacent layers in the 40-PMAA hydrogel and, therefore, a greater density of cross-links in the PMAA-poor strata relative to the 280-PMAA hydrogel, allowing more significant swelling of these stacks in the 280-PMAA hydrogel. The higher density of PMAA chains in the PMAA-poor strata for 40-PMAA is consistent with the thinner PVPON layers adsorbed in the 40-PVPON/PMAA compared to the 280-PVPON/PMAA template films (Figure 2, Table 1) implying less free space available for the chain stretching and PMAA network expansion. The resulting differential expansion of the PMAA hydrogel strata in solution manifests in different elastic moduli and hydration of comparable samples studied with AFM.

Earlier, Hoshino et al. explored the dependence of hydrogel network elasticity as a function of swelling ratio for extreme swelling states.[83] The model PEG hydrogel was obtained from tetra-PEG monomers via cross-end coupling. The bulk PEG hydrogel with a homogeneous distribution of chains and cross-links was rendered ionizable through linear anionic polyelectrolyte chains physically trapped in or grafted to the PEG network. The study reported the relationship between the gel elastic modulus, E, and the hydrogel volumetric swelling ratio, Q, defined through the network thickness swelling ratio as $Q = (t/t_0)^3$, where t and t_0 are the thicknesses of the swollen and as-prepared gels, respectively. The relationship scales as $E \sim Q^{-0.3}$ when $Q < 20$ and when applied to our data (Table 2) predict much softer (10−100 times) PMAA hydrogels in their low-swelling states at pH = 5 or pH = 6.5 than is observed in our work. Apparently, the hierarchical PMAA polyelectrolyte hydrogel architecture consisting of alternating stacks of PMAA-rich and PMAA-poor strata, where the density of cross-links within PMAA-rich strata is greater than that in PMAA-poor strata, may require different modeling treatments and would be interesting to explore further.

https://doi.org/10.1021/acs.macromol.3c01253
Macromolecules XXXX, XXX, XXX−XXX

Table 3. Thickness and Young's Modulus of Dipped and SA $(40\text{-PMAA})_n$ and $(280\text{-PMAA})_n$ Surface Multilayer Hydrogel Films in the Dry State and Solution at pH 5 and pH 6.5 (0.01 M Phosphate Buffer; Equilibrated for 20 min)

	thickness (nm)			Young's modulus		
	dry	pH 5	pH 6.5	dry (GPa)	pH 5 (MPa)	pH 6.5 (MPa)
SA $(40\text{-PMAA})_{40}$	98 ± 3	232 ± 2	393 ± 2	2.1 ± 0.3	51 ± 5	6 ± 1
dipped $(40\text{-PMAA})_{20}$	80 ± 1	175 ± 1	274 ± 2	2.4 ± 0.3	68 ± 3	10 ± 1
SA $(280\text{-PMAA})_{40}$	125 ± 2	482 ± 3	770 ± 2	2.7 ± 0.4	3.4 ± 0.3	0.85 ± 0.05
dipped $(280\text{-PMAA})_{25}$	117 ± 4	345 ± 3	506 ± 2	2.1 ± 0.4	8 ± 1	1.5 ± 0.2

Effect of Polymer Intermixing on (PMAA) Multilayer Hydrogel Mechanical Properties. Our previous work demonstrated that unlike the disordered dipped PMAA multilayer hydrogel, where layering decays rapidly with distance from the surface, SA PMAA multilayer hydrogels display well-defined PMAA strata in the hydrated state.[40,44,56] The dipped PMAA hydrogels, both dry and in solution, feature increased layer interpenetration and an absence of well-defined stratification, unlike the SA PMAA hydrogels.[40,56] Therefore, as observed for SA PMAA hydrogels made with 40-PVPON or 280-PVPON, this difference in polymer layer intermixing should also strongly affect the mechanical response of dipped (highly intermixed) hydrogels.

To test the effect of different PMAA layer intermixing on PMAA hydrogel mechanical properties, we synthesized dipped and SA (PMAA) multilayer hydrogels with similar thicknesses and cross-linking degrees as in an earlier study[44] and measured the Young's modulus for dry and hydrated hydrogel films.

Since dipped (PVPON/PMAA) multilayers exhibit greater bilayer thicknesses, 40-bilayer SA 40-PMAA and 20-bilayer dipped 40-PMAA hydrogels were synthesized to obtain coatings with similar dry thicknesses of 98 ± 3 and 80 ± 1 nm, respectively (Table 3). For the 280-PMAA hydrogel film, the dry thicknesses of the SA and dipped hydrogel coatings were 125 ± 2 and 117 ± 4 nm for 40-bilayer SA 280-PMAA and 25-bilayer dipped 280-PMAA hydrogels, respectively (Table 3).

Figure 8 shows that Young's modulus maps for dry dipped 40-PMAA (Figure 8a) and 280-PMAA (Figure 8b) hydrogel

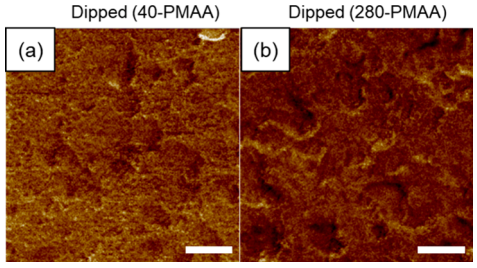

Figure 8. Young's modulus maps of dry dipped (a) $(40\text{-PMAA})_{20}$ and (b) $(280\text{-PMAA})_{25}$ surface multilayer hydrogel films as analyzed by AFM nanoindentation. The scale bar is 200 nm.

coatings exhibited homogeneous elasticity over 1 μm^2 areas with the average elasticity moduli of 2.4 ± 0.3 and 2.1 ± 0.4 GPa for dipped 40-PMAA and 280-PMAA hydrogels, respectively (Table 3), being similar for both dipped hydrogels regardless of the PVPON molecular weight used for their fabrication (Table 3). Moreover, these elasticity modulus values were similar to those measured for SA PMAA dry hydrogel films, with the average Young's modulus values of 2.1 ± 0.3 and 2.7 ± 0.4 GPa found for SA (40-PMAA) and SA (280-PMAA) hydrogels, respectively (Table 3).

When the 40-PMAA hydrogels were submerged in solution at pH 5, the SA hydrogel swelled more than the dipped (40-PMAA) hydrogel despite their similar dry thicknesses with swelling ratios of 2.4 ± 0.1 and 2.2 ± 0.1 for the SA and dipped 40-PMAA hydrogels, respectively (Table 3, Figure 9a). A

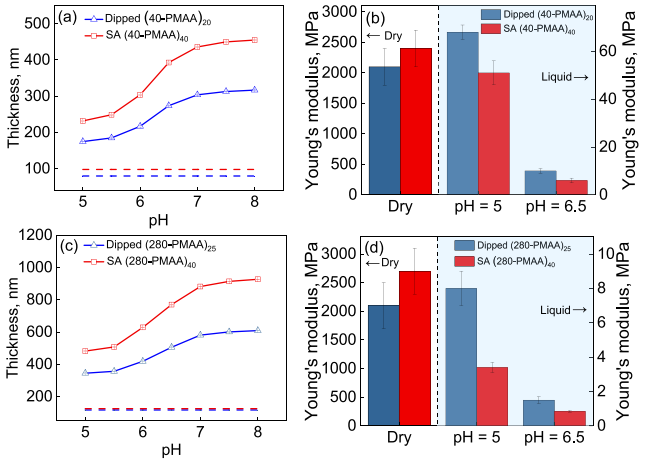

Figure 9. pH-dependent swelling of (a) 40-PMAA and (c) 280-PMAA multilayer hydrogels obtained via dipping (triangles) or SA (squares) multilayer assembly and measured by *in situ* ellipsometry. (b, d) Average Young's modulus of (b) 40-PMAA and (d) 280-PMAA multilayer hydrogels obtained via dipped or SA LbL assembly as measured by AFM nanoindentation. Dashed lines show the dry thicknesses of the corresponding PMAA hydrogel films.

different trend was observed when the hydrogels were immersed in pH 6.5 solutions, where the SA 40-PMAA hydrogel showed a greater swelling ratio of 4.0 ± 0.1 compared to 3.4 ± 0.1 for the dipped 40-PMAA hydrogel (Table 3, Figure 9a).

Despite similar Young's moduli found for dry dipped and SA 40-PMAA hydrogel films, the hydrated hydrogels' elasticity was significantly different. For example, Young's modulus of the dipped 40-PMAA hydrogel was 1.3-fold higher than that of the SA 40-PMAA hydrogel (Table 3, Figure 9b), consistent with the different swelling ratios reported above. The lesser swelling of dipped PMAA multilayer hydrogels at pH 7.5, compared to their SA counterparts, has been reported previously by our group and was explained by a higher degree of PMAA chain interdiffusion and intermixing during dipping.[44]

Increasing solution pH further softened both dipped and SA 40-PMAA hydrogels due to increased PMAA-ionization-enhanced swelling of the network. The elasticity of the 40-PMAA hydrogel decreased from 68 ± 3 MPa at pH 5 to 10 ± 1 MPa at pH 6.5 for the dipped network and from 51 ± 5 MPa at pH 5 to 6 ± 1 MPa at pH 6.5 for the SA network (Figure

https://doi.org/10.1021/acs.macromol.3c01253
Macromolecules XXXX, XXX, XXX−XXX

9b). Therefore, although the dipped hydrogel swelling was only 1.2 times smaller than that of the SA hydrogel at pH 6.5, the dipped 40-PMAA hydrogel was 1.7-fold more rigid than its SA counterpart, consistent with the hypothesis of internal hydrogel structure affecting swelling and mechanical properties.

When comparing dipped and SA 280-PMAA hydrogel mechanical responses in solution, we observed softening of the SA 280-PMAA hydrogel compared to the dipped 280-PMAA hydrogel similar to what was seen in the 40-PMAA network. Dipped and SA 280-PMAA hydrogel films in the dry state exhibited Young's moduli in the range of 2−3 GPa (Table 3, Figure 9d) but softened dramatically upon hydration. Specifically, the SA 280-PMAA hydrogel swelled 3.9 ± 0.1 and 6.2 ± 0.1 times at pH 5 and 6.5, respectively, while the dipped 280-PMAA hydrogel showed a smaller degree of swelling of 3.0 ± 0.1 at pH 5 and 4.3 ± 0.2 at pH 6.5 (Table 3, Figure 9c). Likewise, the average elasticity modulus of the 280-PMAA hydrogel decreased to 8 ± 1 MPa for the dipped network and to a lower value of 3.4 ± 0.3 MPa for the SA 280-PMAA hydrogel at pH 5 (Table 3, Figure 9d). Dipped and SA 280-PMAA hydrogels also demonstrated further softening in solution at pH 6.5 with corresponding elasticity values of 1.5 ± 0.2 MPa for the dipped hydrogel and 0.85 ± 0.05 MPa for SA 280-PMAA, respectively. These data demonstrate that an SA 280-PMAA hydrogel of similar thickness and cross-linking degree has 1.8 times smaller Young's modulus than a dipped 280-PMAA hydrogel (Figure 9d).

Our mechanical response data suggest that more rigid dipped PMAA multilayer hydrogels are obtained regardless of the molecular weight of PVPON (Figure 9b,d). More homogeneous chain intermixing in the template dipped multilayer coatings and, subsequently, a more uniform cross-link distribution reduces the effect of cross-link-poor strata and so reduces the hydrogel's "free space", leading to reduced network expansion and a higher Young's modulus. Similarly, a greater degree of component intermixing and physical chain entanglements was observed in tannic acid/PVPON multilayer capsules when a polycationic surface primer poly(ethylene imine) was used. This increased component intermixing registered as increased surface roughening and was identified as the cause of capsule shell stiffening and increased Young's modulus relative to counterparts lacking a priming polycation.[48]

CONCLUSIONS

In this work, we explored the effect of the internal organization of PMAA multilayer hydrogel coatings on their mechanical properties. The PMAA hydrogel films were synthesized by cross-linking PMAA in PVPON/PMAA hydrogen-bonded multilayer templates obtained by dipped or SA assembly of polymers at surfaces using a sacrificial PVPON binding layer with two different molecular weights of 40,000 and 280,000 g mol^{-1}. The thicknesses of the cross-linked 40-PMAA and 280-PMAA multilayer hydrogels demonstrated a linear dependence on the PMAA layer number with slightly thicker layers seen in 280-PMAA. ATR-FTIR analysis confirmed that cross-link densities of the SA PMAA surface-attached hydrogels obtained using 40-PVPON and 280-PVPON were similar. Despite this equivalence, SA 280-PMAA multilayer hydrogels consistently showed about 30% greater swelling at pH 6.5 in comparison to SA 40-PMAA hydrogels. *In situ* spectroscopic ellipsometry and NR analysis of SA PMAA hydrogel swelling revealed greater hydration of SA 280-PMAA versus 40-PMAA with the number of D_2O molecules associated with each monomer in the swollen hydrogel being 8.2 ± 0.1 and 9.6 ± 0.2 for $(40\text{-PMAA})_{20}$ and $(280\text{-PMAA})_{20}$, respectively, at pH 5, and 9.8 ± 0.1 and 12.2 ± 0.2 for $(40\text{-PMAA})_{20}$ and $(280\text{-PMAA})_{20}$, respectively, at pH 6.55. A similar trend was found for the number of D_2O molecules per unit of hydrogel volume, showing an increase from 23.5 ± 0.3 D_2O molecules per nm^3 for $(40\text{-PMAA})_{20}$ to 25.3 ± 0.5 for $(40\text{-PMAA})_{20}$ at pH 5 and from 25.0 ± 0.4 for $(40\text{-PMAA})_{20}$ to 27.2 ± 0.6 D_2O molecules per nm^3 for the (280-pMAA) hydrogel at pH 6.5. Hydration of SA (PMAA) hydrogels was accompanied by increased surface roughness due to polymer chain relaxation through chain untangling and loop extension during network hydration, with more than 30% higher roughness observed for the SA PMAA hydrogel obtained through assembly of PVPON of larger molecular weight. We analyzed the mechanical properties of the SA PMAA multilayer hydrogels in dry and hydrated states by AFM nanoindentation using a colloidal probe. The Young's modulus of the dry SA PMAA film was homogeneous over 1 μm^2 areas and was similar for SA and dipped (PMAA) hydrogels regardless of the molecular weight of the sacrificial PVPON used in fabrication, ranging from 2.0 ± 0.1 to 2.7 ± 0.4 GPa. Remarkably, upon swelling in solution, the SA 280-PMAA hydrogel was softer than its 40-PMAA counterpart with an approximately threefold lower Young's modulus of 15 ± 1 MPa in solution at pH 5 and 2 ± 0.1 MPa at pH 6.5 compared to the SA 40-PMAA multilayer hydrogel. This difference in swelling of the SA PMAA hydrogels made from a sacrificial binder with different molecular weights was explained via a varying density of cross-links throughout the PMAA hydrogel consisting of a network of alternating cross-link-rich (the original PMAA layers) and cross-link-poor PMAA strata, centered between adjacent PMAA layers in the cross-linked hydrogel where templating PVPON layers were located. Our ellipsometry and NR data suggest that controlling the density of cross-links between PMAA strata in PMAA multilayer hydrogels by changing the molecular weight of templating PVPON results in a different swelling of the PMAA hydrogel. The greater intermixing of PMAA chains in the PMAA-poor strata for 40-PMAA is consistent with less PVPON adsorbed in the 40-PVPON/PMAA template than in the 280-PVPON/PMAA template, implying less free space available for chain stretching and PMAA network expansion. The resultant differential expansion of the PMAA hydrogel strata in solution leads to different elastic moduli and hydration of the same hydrogel made with PVPON with different molecular weights.

We have also confirmed that the difference in PMAA layer intermixing explains the difference in the mechanical response of the dipped (highly intermixed) and SA (well-organized, less-intermixed) PMAA multilayer hydrogels. We have found that despite exhibiting similar rigidity for dry dipped and SA 40-PMAA films, the hydrated (pH 5) hydrogels' elasticity was significantly different with the Young's modulus of the dipped 40-PMAA hydrogel being 1.3-fold higher than that for the SA 40-PMAA hydrogel at pH 5, consistent with their different swelling ratios observed by ellipsometry and NR. Increasing the solution pH to 6.5 further softened dipped and SA PMAA hydrogels, with the dipped 40-PMAA hydrogel being 1.7-fold more rigid than its SA counterpart. In the case of 280-PMAA hydrogels, the SA hydrogel of the same thickness and cross-linking degree had a 1.8-fold lower Young's modulus than the

https://doi.org/10.1021/acs.macromol.3c01253
Macromolecules XXXX, XXX, XXX−XXX

dipped 280-PMAA hydrogel. The hydrogel nanoindentation data demonstrated that more rigid dipped PMAA multilayer hydrogels are obtained regardless of the molecular weight of PVPON, and greater chain intermixing in the dipped hydrogel reduces the hydrogel's "free space", leading to reduced network expansion and a higher Young's modulus. Our study demonstrates that the properties of pH-responsive multilayer hydrogels are sensitive to nanostructured internal organization and selective modulation of the cross-link density within the PMAA hydrogel strata. This controlled polymer chain intermixing makes possible the synthesis of hydrogel materials with finely tuned hydrogel internal architectures and precisely controlled physical properties, such as hydrogel swelling, surface morphology, and mechanical response, which are essential for these materials' applications in sensing, drug delivery, and tissue engineering.

■ ASSOCIATED CONTENT

Supporting Information

The Supporting Information is available free of charge at https://pubs.acs.org/doi/10.1021/acs.macromol.3c01253.

Constrained model of NR data; GPC chromatographs of PVPON with M_w 40,000 and 280,000 g mol^{-1}; an incremental growth of PMAA/PVPON hydrogen-bonded multilayers; an average thickness distribution of PMAA and PVPON in $(PMAA/PVPON)_{10}$ films; *in situ* ATR-FTIR spectra of $(PVPON/PMAA)_{10.5}$, EDC-activated $(PVPON/PMAA)_{10.5}$, and $(PMAA)_{10.5}$ hydrogel coatings; ATR-FTIR deconvoluted spectra of $(40\text{-}PMAA)_{10.5}$ and $(280\text{-}PMAA)_{10.5}$ hydrogels; AFM topography images of 40-bilayer (40-PVPON/PMAA) and (280-PVPON/PMAA) hydrogen-bonded and (40-PMAA) and (280-PMAA) multilayer hydrogel coatings in dry and wet states (pH 5 and 6.5); and roughness of 40-bilayer (40-PVPON/PMAA) and (280-PVPON/PMAA) hydrogen-bonded and (40-PMAA) and (280-PMAA) multilayer hydrogel coatings (PDF)

■ AUTHOR INFORMATION

Corresponding Authors

John F. Ankner − *Second Target Station Project, Oak Ridge National Laboratory, Oak Ridge, Tennessee 37831, United States;* orcid.org/0000-0002-6737-5718; Email: anknerjf@ornl.gov

Eugenia Kharlampieva − *Department of Chemistry, Center for Nanoscale Materials and Biointegration, University of Alabama at Birmingham, Birmingham, Alabama 35294, United States;* orcid.org/0000-0003-0227-0920; Email: ekharlam@uab.edu

Authors

Maksim Dolmat − *Department of Chemistry, Center for Nanoscale Materials and Biointegration, University of Alabama at Birmingham, Birmingham, Alabama 35294, United States;* orcid.org/0000-0002-4918-7342

Veronika Kozlovskaya − *Department of Chemistry, Center for Nanoscale Materials and Biointegration, University of Alabama at Birmingham, Birmingham, Alabama 35294, United States;* orcid.org/0000-0001-9089-4842

Complete contact information is available at: https://pubs.acs.org/10.1021/acs.macromol.3c01253

Author Contributions

[§]M.D. and V.K. contributed equally.

Notes

The authors declare no competing financial interest.

■ ACKNOWLEDGMENTS

This work was funded by NSF DMR award no. 1904816. Measurements at Oak Ridge National Laboratory and work by J.F.A. were carried out under UT-Battelle, LLC, under Contract No. DE-AC05-00OR22725 with the US Department of Energy. This material is partly based upon work supported under the IR/D Program by the National Science Foundation (E.K.). Any opinions, findings, conclusions, or recommendations expressed in this material are those of the author(s) and do not necessarily reflect the views of the National Science Foundation.

■ REFERENCES

(1) Culver, H. R.; Clegg, J. R.; Peppas, N. A. Analyte-Responsive Hydrogels: Intelligent Materials for Biosensing and Drug Delivery. *Acc. Chem. Res.* **2017**, *50*, 170−178.

(2) Li, J.; Mooney, D. Designing Hydrogels for Controlled Drug Delivery. *Nat. Rev. Mater.* **2016**, *1*, 16071 DOI: 10.1038/natrevmats.2016.71.

(3) Merkel, T. J.; Jones, S. W.; Herlihy, K. P.; Kersey, F. R.; Shields, A. R.; Napier, M.; Luft, J. C.; Wu, H.; Zamboni, W. C.; Wang, A. Z.; Bear, J. E.; DeSimone, J. M. Using Mechanobiological Mimicry of Red Blood Cells to Extend Circulation Times of Hydrogel Microparticles. *Proc. Natl. Acad. Sci.* **2011**, *108*, 586−591.

(4) Vashahi, F.; Martinez, M. R.; Dashtimoghadam, E.; Fahimipour, F.; Keith, A. M.; Bersenev, E. A.; Ivanov, D. A.; Zhulina, E. B.; Popryadukhin, P.; Matyjaszewski, K.; Vatankhah-Varnosfaderani, M.; Sheiko, S. S. Injectable bottlebrush hydrogels with tissue-mimetic mechanical properties. *Sci. Adv.* **2022**, *8*, No. eabm2469.

(5) Bittner, S. M.; Pearce, H. A.; Hogan, K. J.; Smoak, M. M.; Guo, J. L.; Melchiorri, A. J.; Scott, D. W.; Mikos, A. G. Swelling Behaviors of 3D Printed Hydrogel and Hydrogel-Microcarrier Composite Scaffolds. *Tissue Eng., Part A* **2021**, *27*, 665−678.

(6) Kudryavtseva, V.; Otero, M.; Zhang, J.; Bukatin, A.; Gould, D.; Sukhorukov, G. B. Drug-Eluting Sandwich Hydrogel Lenses Based on Microchamber Film Drug Encapsulation. *ACS Nanosci. Au* **2023**, *3*, 256−265.

(7) Caccavo, D.; Cascone, S.; Lamberti, G.; Barba, A. A. Hydrogels: Experimental Characterization and Mathematical Modelling of Their Mechanical and Diffusive Behavior. *Chem. Soc. Rev.* **2018**, *47*, 2357−2373.

(8) Means, A. K.; Ehrhardt, D. A.; Whitney, L. V.; Grunlan, M. A. Thermoresponsive Double Network Hydrogels with Exceptional Compressive Mechanical Properties. *Macromol. Rapid Commun.* **2017**, *38*, 1700351.

(9) Lin, X.; Zhao, X.; Xu, C.; Wang, L.; Xia, Y. Progress in the Mechanical Enhancement of Hydrogels: Fabrication Strategies and Underlying Mechanisms. *J. Polym. Sci.* **2022**, *60*, 2525−2542.

(10) Khutoryanskaya, O. V.; Mayeva, Z. A.; Mun, G. A.; Khutoryanskiy, V. V. Designing Temperature-Responsive Biocompatible Copolymers and Hydrogels Based on 2-Hydroxyethyl(meth)acrylates. *Biomacromolecules* **2008**, *9*, 3353−3361.

(11) Onat, B.; Ulusan, S.; Banerjee, S.; Erel-Goktepe, I. Multifunctional layer-by-layer modified chitosan/poly(ethylene glycol) hydrogels. *Eur. Polym. J.* **2019**, *112*, 73−86.

(12) Flory, P. J.; Rehner, J. Statistical mechanics of cross-linked polymer networks. II Swelling. *J. Chem. Phys.* **1943**, *11*, 521−526.

(13) Longo, G. S.; Olvera de la Cruz, M.; Szleifer, I. Molecular Theory of Weak polyelectrolyte Gels: The Role of pH and Salt Concentration. *Macromolecules* **2011**, *44*, 147−158.

(14) Means, A. K.; Shrode, C. S.; Whitney, L. V.; Ehrhardt, D. A.; Grunlan, M. A. Double Network Hydrogels that Mimic the Modulus,

Strength, and Lubricity of Cartilage. *Biomacromolecules* **2019**, *20*, 2034−2042.
(15) Ahearne, M. Introduction to Cell-Hydrogel Mechanosensing. *Interface Focus* **2014**, *4*, 20130038.
(16) Jiang, L.; He, S.; Liu, A.; Zhang, J.; Liu, J.; He, S.; Shao, W. Preparation and Characterization of Self-Healable and Wearable Hydrogels with Ultrasensitive Sensing Performances. *Composites, Part B* **2022**, *239*, No. 109982.
(17) Danielsen, S. P. O.; Beech, H. K.; Wang, S.; El-Zaatari, B. M.; Wang, X.; Sapir, L.; Ouchi, T.; Wang, Z.; Johnson, P. N.; Hu, Y.; Lundberg, D. J.; Stoychev, G.; Craig, S. L.; Johnson, J. A.; Kalow, J. A.; Olsen, B. D.; Rubinstein, M. Molecular Characterization of Polymer Networks. *Chem. Rev.* **2021**, *121*, 5042−5092.
(18) Switacz, V. K.; Wypysek, S. K.; Degen, R.; Crassous, J. J.; Spehr, M.; Richtering, W. Influence of Size and Cross-Linking Density of Microgels on Cellular Uptake nd Uptake Kinetics. *Biomacromolecules* **2020**, *21*, 4532−4544.
(19) Best, J. P.; Javed, S.; Richardson, J. J.; Cho, K. L.; Kamphuis, M. M. J.; Caruso, F. Stiffness-Mediated Adhesion of Cervical Cancer Cells to Soft Hydrogel Films. *Soft Matter* **2013**, *9*, 4580−4584.
(20) Kozlovskaya, V.; Dolmat, M.; Kharlampieva, E. Polymeric Particulates of Controlled Rigidity for Biomedical Applications. *ACS Appl. Polym. Mater.* **2021**, *3*, 2274−2289.
(21) Li, J.; Illeperuma, W. R. K.; Suo, Z.; Vlassak, J. J. Hybrid Hydrogels with Extremely High Stiffness and Toughness. *ACS Macro Lett.* **2014**, *3*, 520−523.
(22) Lee, S. B.; Kim, Y. H.; Chong, M. S.; Hong, S. H.; Lee, Y. M. Study of Gelatin-Containing Artificial Skin v: Fabrication of Gelatin Scaffolds Using a Salt-Leaching Method. *Biomaterials* **2005**, *26*, 1961−1968.
(23) Baker, B. M.; Trappmann, B.; Wang, W. Y.; Sakar, M. S.; Kim, I. L.; Shenoy, V. B.; Burdick, J. A.; Chen, C. S. Cell-Mediated Fibre Recruitment Drives Extracellular Matrix Mechanosensing in Engineered Fibrillar Microenvironments. *Nat. Mater.* **2015**, *14*, 1262−1268.
(24) Wu, X.; Black, L.; Santacana-Laffitte, G.; Patrick, C. W. Preparation and Assessment of Glutaraldehyde-Crosslinked Collagen−Chitosan Hydrogels for Adipose Tissue Engineering. *J. Biomed. Mater. Res., Part A* **2007**, *81A*, 59−65.
(25) Ji, C.; Annabi, N.; Khademhosseini, A.; Dehghani, F. Fabrication of Porous Chitosan Scaffolds for Soft Tissue Engineering Using Dense Gas CO2. *Acta Biomater.* **2011**, *7*, 1653−1664.
(26) Richbourg, N. R.; Wancura, M.; Gilchrist, A. E.; Toubbeh, S.; Harley, B. A. C.; Cosgriff-Hernandez, E.; Peppas, N. A. Precise Control of Synthetic Hydrogel Network Structure via Linear, Independent Synthesis-Swelling Relationships. *Sci. Adv.* **2021**, *7*, No. eabe3245.
(27) Annabi, N.; Nichol, J. W.; Zhong, X.; Ji, C.; Koshy, S.; Khademhosseini, A.; Dehghani, F. Controlling the Porosity and Microarchitecture of Hydrogels for Tissue Engineering. *Tissue Eng., Part B* **2010**, *16*, 371−383.
(28) Souza Almeida, F.; Guedes Silva, K. C.; Matias Navarrete de Toledo, A.; Kawazoe Sato, A. C. Modulating Porosity and Mechanical Properties of Pectin Hydrogels by Starch Addition. *J. Food Sci. Technol.* **2021**, *58*, 302−310.
(29) Lee, M. K.; Rich, M. H.; Baek, K.; Lee, J.; Kong, H. Bioinspired Tuning of Hydrogel Permeability-Rigidity Dependency for 3D Cell Culture. *Sci. Rep.* **2015**, *5*, 8948.
(30) Tibbitt, M. W.; Kloxin, A. M.; Sawicki, L. A.; Anseth, K. S. Mechanical Properties and Degradation of Chain and Step-Polymerized Photodegradable Hydrogels. *Macromolecules* **2013**, *46*, 2785−2792.
(31) Choi, S.; Kim, J. Designed Fabrication of Super-Stiff, Anisotropic Hybrid Hydrogels via Linear Remodeling of Polymer Networks and Subsequent Crosslinking. *J. Mater. Chem. B* **2015**, *3*, 1479−1483.
(32) Zarket, B. C.; Raghavan, S. R. Onion-like Multilayered Polymer Capsules Synthesized by a Bioinspired inside-out Technique. *Nat. Commun.* **2017**, *8*, 193.
(33) Xie, Q.; Zhuang, Y.; Ye, G.; Wang, T.; Cao, Y.; Jiang, L. Astral Hydrogels Mimic Tissue Mechanics by Aster-Aster Interpenetration. *Nat. Commun.* **2021**, *12*, 4277.
(34) Hua, M.; Wu, S.; Ma, Y.; Zhao, Y.; Chen, Z.; Frenkel, I.; Strzalka, J.; Zhou, H.; Zhu, X.; He, X. Strong Tough Hydrogels via the Synergy of Freeze-Casting and Salting Out. *Nature* **2021**, *590*, 594−599.
(35) Kozlovskaya, V.; Kharlampieva, E.; Erel, I.; Sukhishvili, S. A. Multilayer-Derived, Ultrathin, Stimuli-Responsive Hydrogels. *Soft Matter* **2009**, *5*, 4077−4087.
(36) Selin, V.; Ankner, J. F.; Sukhishvili, S. A. Nonlinear Layer-by-Layer Films: Effects of Chain Diffusivity on Film Structure and Swelling. *Macromolecules* **2017**, *50*, 6192−6201.
(37) Picart, C.; Mutterer, J.; Richert, L.; Luo, Y.; Prestwich, G. D.; Schaaf, P.; Voegel, J. C.; Lavalle, P. Molecular basis for the explanation of the exponential growth of polyelectrolyte multilayers. *Proc. Natl. Acad. Sci.* **2002**, *99*, 12531−12535.
(38) Xu, L.; Pristinski, D.; Zhuk, A.; Stoddart, C.; Ankner, J. F.; Sukhishvili, S. A. Linear versus Exponential Growth of Weak polyelectrolyte Multilayers: Correlation with polyelectrolyte Complexes. *Macromolecules* **2012**, *45*, 3892−3901.
(39) Espinosa-Dzib, A.; Chen, J.; Zavgorodnya, O.; Kozlovskaya, V.; Liang, X.; Kharlampieva, E. Tuning Assembly and Enzymatic Degradation of Silk/Poly(N-Vinylcaprolactam) Multilayers via Molecular Weight and Hydrophobicity. *Soft Matter* **2015**, *11*, 5133−5145.
(40) Kozlovskaya, V.; Stockmal, K. A.; Higgins, W.; Ankner, J. F.; Morgan, S. E.; Kharlampieva, E. Architecture of Hydrated Multilayer Poly(Methacrylic Acid) Hydrogels: The Effect of Solution pH. *ACS Appl. Polym. Mater.* **2020**, *2*, 2260−2273.
(41) Liu, G.; Zou, S.; Fu, L.; Zhang, G. Roles of Chain Conformation and Interpenetration in the Growth of a polyelectrolyte Multilayer. *J. Phys. Chem. B* **2008**, *112*, 4167−4171.
(42) Selin, V.; Ankner, J.; Sukhishvili, S. Ionically Paired Layer-By-Layer Hydrogels: Water and polyelectrolyte Uptake Controlled by Deposition Time. *Gels* **2018**, *4*, 7.
(43) Lösche, M.; Schmitt, J.; Decher, G.; Bouwman, W. G.; Kjaer, K. Detailed Structure of Molecularly Thin polyelectrolyte Multilayer Films on Solid Substrates as Revealed by Neutron Reflectometry. *Macromolecules* **1998**, *31*, 8893−8906.
(44) Kozlovskaya, V.; Zavgorodnya, O.; Wang, Y.; Ankner, J. F.; Kharlampieva, E. Tailoring Architecture of Nanothin Hydrogels: Effect of Layering on pH-Triggered Swelling. *ACS Macro Lett.* **2013**, *2*, 226−229.
(45) Xu, L.; Selin, V.; Zhuk, A.; Ankner, J. F.; Sukhishvili, S. A. Molecular Weight Dependence of Polymer Chain Mobility Within Multilayer Films. *ACS Macro Lett.* **2013**, *2*, 865−868.
(46) Shen, L.; Chaudouet, P.; Ji, J.; Picart, C. pH-Amplified Multilayer Films Based on Hyaluronan: Influence of HA Molecular Weight and Concentration on Film Growth and Stability. *Biomacromolecules* **2011**, *12*, 1322−1331.
(47) Alkekhia, D.; Shukla, A. Influence of Poly-L-Lysine Molecular Weight on Antibacterial Efficacy in Polymer Multilayer Films. *J. Biomed. Mater. Res., Part A* **2019**, *107*, 1324−1339.
(48) Lisunova, M. O.; Drachuk, I.; Shchepelina, O. A.; Anderson, K. D.; Tsukruk, V. V. Direct Probing of Micromechanical Properties of Hydrogen-Bonded Layer-By-Layer Microcapsule Shells with Different Chemical Compositions. *Langmuir* **2011**, *27*, 11157−11165.
(49) Jang, Y.; Seo, J.; Akgun, B.; Satija, S.; Char, K. Molecular Weight Dependence on the Disintegration of Spin-Assisted Weak polyelectrolyte Multilayer Films. *Macromolecules* **2013**, *46*, 4580−4588.
(50) Ghoussoub, Y. E.; Zerball, M.; Fares, H. M.; Ankner, J. F.; von Klitzing, R.; Schlenoff, J. B. Ion Distribution in Dry polyelectrolyte Multilayers: A Neutron Reflectometry Study. *Soft Matter* **2018**, *14*, 1699−1708.
(51) Kellogg, G. J.; Mayes, A. M.; Stockton, W. B.; Ferreira, M.; Rubner, M. F.; Satija, S. K. Neutron Reflectivity Investigations of Self-

https://doi.org/10.1021/acs.macromol.3c01253
Macromolecules XXXX, XXX, XXX−XXX

Assembled Conjugated Polyion Multilayers. *Langmuir* **1996**, *12*, 5109−5113.
(52) Schmitt, J.; Gruenewald, T.; Decher, G.; Pershan, P. S.; Kjaer, K.; Loesche, M. Internal Structure of Layer-by-Layer Adsorbed polyelectrolyte Films: A Neutron and X-ray Reflectivity Study. *Macromolecules* **1993**, *26*, 7058−7063.
(53) Gresham, I. J.; Reurink, D. M.; Prescott, S. W.; Nelson, A. R. J.; de Vos, W. M.; Willott, J. D. Structure and Hydration of Asymmetric polyelectrolyte Multilayers as Studied by Neutron Reflectometry: Connecting Multilayer Structure to Superior Membrane Performance. *Macromolecules* **2020**, *53*, 10644−10654.
(54) Kozlovskaya, V.; Ankner, J. F.; O'Neill, H.; Zhang, Q.; Kharlampieva, E. Localized entrapment of green fluorescent protein within nanostructured polymer films. *Soft Matter* **2011**, *7*, 11453−11463.
(55) Cho, J.; Char, K.; Hong, J.-D.; Lee, K.-B. Fabrication of highly ordered multilayer films using a spin self-assembly method. *Adv. Mater.* **2001**, *13*, 1076.
(56) Kozlovskaya, V.; Zavgorodnya, O.; Ankner, J. F.; Kharlampieva, E. Controlling internal organization of multilayer poly(methacrylic acid) hydrogels with polymer molecular weight. *Macromolecules* **2015**, *48*, 8585−8593.
(57) Gao, C.; Donath, E.; Moya, S.; Dudnik, V.; Möhwald, H. Elasticity of Hollow polyelectrolyte Capsules Prepared by the Layer-By-Layer Technique. *Eur. Phys. J. E* **2001**, *5*, 21−27.
(58) Lulevich, V. V.; Nordschild, S.; Vinogradova, O. I. Investigation of Molecular Weight and Aging Effects on the Stiffness of polyelectrolyte Multilayer microcapsules. *Macromolecules* **2004**, *37*, 7736−7741.
(59) Dyck, M.; Krüger, P.; Lösche, M. Headgroup organization and hydration of methylated phosphatidylethanolamines in Langmuir monolayers. *Phys. Chem. Chem. Phys.* **2005**, *7*, 150−156.
(60) Sidorenko, A.; Krupenkin, T.; Aizenberg, J. Controlled Switching of the Wetting Behavior of Biomimetic Surfaces with Hydrogel-Supported Nanostructures. *J. Mater. Chem.* **2008**, *18*, 3841−3846.
(61) Kozlovskaya, V.; Higgins, W.; Chen, J.; Kharlampieva, E. Shape Switching of Hollow Layer-by-Layer Hydrogel Microcontainers. *ChemComm.* **2011**, *47*, 8352−8354.
(62) Wang, Y.; Kozlovskaya, V.; Arcibal, I. G.; Cropek, D. M.; Kharlampieva, E. Highly Swellable Ultrathin Poly(4-Vinylpyridine) Multilayer Hydrogels with pH-Triggered Surface Wettability. *Soft Matter* **2013**, *9*, 9420−9429.
(63) Dokukin, M. E.; Sokolov, I. Quantitative Mapping of the Elastic Modulus of Soft Materials with HarmoniX and PeakForce QNM AFM modes. *Langmuir* **2012**, *28*, 16060−16071.
(64) Knappe, P.; Bienert, R.; Weidner, S.; Thünemann, A. F. Characterization of poly(N-vinyl-2-pyrrolidone)s with broad size distributions. *Polymer* **2010**, *51*, 1723−1727.
(65) Schneider, A.; Francius, G.; Obeid, R.; Schwinte, P.; Hemmerle, J.; Frisch, B.; Schaaf, P.; Voegel, L.-C.; Senger, B.; Picart, C. polyelectrolyte Multilayers with a Tunable Young's Modulus: Influence of Film Stiffness on Cell Adhesion. *Langmuir* **2006**, *22*, 1193−1200.
(66) Ji, Y.; Yang, X.; Ji, Z.; Zhu, L.; Ma, N.; Chen, D.; Jia, X.; Tang, J.; Cao, Y. DFT-Calculated IR Spectrum Amide I, II, and III Band Contributions of N-Methylacetamide Fine Components. *ACS Omega* **2020**, *5*, 8572−8578.
(67) Kharlampieva, E.; Erel-Unal, I.; Sukhishvili, S. A. Amphoteric Surface hydrogels derived from hydrogen-bonded multilayers: Reversible loading of dyes and proteins. *Langmuir* **2007**, *23*, 175−181.
(68) Kozlovskaya, V.; Kharlampieva, E.; Mansfield, M. L.; Sukhishvili, S. A. Poly(Methacrylic Acid) Hydrogel Films and Capsules: Response to pH and Ionic Strength, and Encapsulation of Macromolecules. *Chem. Mater.* **2006**, *18*, 328−336.
(69) Toomey, R.; Freidank, D.; Ruehe, J. Swelling Behavior of Thin, Surface-Attached Polymer Networks. *Macromolecules* **2004**, *37*, 882−887.
(70) Harms, S.; Rätzke, K.; Faupel, F.; Egger, W.; Ravello, L.; Laschewsky, A.; Wang, W.; Müller-Buschbaum, P. Free Volume and Swelling in Thin Films of Poly(N-isopropylacrylamide) End-Capped with n-Butyltrithiocarbonate. *Macromol. Rapid Commun.* **2010**, *31*, 1364−1367.
(71) Higgins, W.; Kozlovskaya, V.; Alford, A.; Ankner, J.; Kharlampieva, E. Stratified temperature-responsive multilayer hydrogels of poly(N-vinylpyrrolidone) and poly(N-vinylcaprolactam): Effect of hydrogel architecture on properties. *Macromolecules* **2016**, *49*, 6953−6964.
(72) Karoyo, A. H.; Wilson, L. D. A Review on the Design and Hydration Properties of Natural Polymer-Based Hydrogels. *Materials* **2021**, *14*, 1095.
(73) Selin, V.; Albright, V.; Ankner, J. F.; Marin, A.; Andrianov, A. K.; Sukhishvili, S. A. Biocompatible Nanocoatings of Fluorinated Polyphosphazenes through Aqueous Assembly. *ACS Appl. Mater. Interfaces* **2018**, *10*, 9756−9764.
(74) Olejniczak, M. N.; Kozanecki, M.; Saramak, J.; Matusiak, M.; Kadlubowski, S.; Matyjaszewski, K. Raman Spectroscopy Study on Influence of Network Architecture on Hydration of Poly(2-(2-Methoxyethoxy)Ethyl Methacrylate) Hydrogels. *J. Raman Spectrosc.* **2017**, *48*, 465−473.
(75) Amorim, S.; da Costa, D. S.; Freitas, D.; Reis, C. A.; Reis, R. L.; Pashkuleva, I.; Pires, R. A. Molecular Weight of Surface Immobilized Hyaluronic Acid Influences CD44-Mediated Binding of Gastric Cancer Cells. *Sci. Rep.* **2018**, *8*, 16058.
(76) Hayward, R. C.; Chmelka, B. F.; Kramer, E. J. Template Cross-Linking Effects on Morphologies of Swellable Block Copolymer and Mesostructured Silica Thin Films. *Macromolecules* **2005**, *38*, 7768−7783.
(77) Lehaf, A. M.; Hariri, H. H.; Schlenoff, J. B. Homogeneity, Modulus, and Viscoelasticity of polyelectrolyte Multilayers by Nanoindentation: Refining the Buildup Mechanism. *Langmuir* **2012**, *28*, 6348−6355.
(78) Dolmat, M.; Kozlovskaya, V.; Cropek, D.; Kharlampieva, E. Free-standing nanothin hydrogels: Effects of composition and pH-dependent hydration on mechanical properties. *ACS Appl. Polym. Mater.* **2021**, *3*, 3960−3971.
(79) Trenkenschuh, K.; Erath, J.; Kuznetsov, V.; Gensel, J.; Boulmedais, F.; Schaaf, P.; Papastavrou, G.; Fery, A. Tuning of the Elastic Modulus of polyelectrolyte Multilayer Films built up from Polyanions Mixture. *Macromolecules* **2011**, *44*, 8954−8961.
(80) Cheng, X.; Putz, K. W.; Wood, C. D.; Brinson, L. C. Characterization of Local Elastic Modulus in Confined Polymer Films via AFM Indentation. *Macromol. Rapid Commun.* **2015**, *36*, 391−397.
(81) Fery, A.; Tsukruk, V. Tailoring the Mechanics of Freestanding Multilayers. In *Multilayer Thin Films: Sequential Assembly of Nanocomposite Materials*, Second ed.; (Eds. Decher, G.; Schlenoff, J. B.); John Wiley & Sons: 2012, 363−392.
(82) Nolte, A. J.; Rubner, M. F.; Cohen, R. E. Determining the Young's Modulus of polyelectrolyte Multilayer Films via Stress-Induced Mechanical Buckling Instabilities. *Macromolecules* **2005**, *38*, 5367−5370.
(83) Hoshino, K.; Nakajima, T.; Matsuda, T.; Sakai, T.; Gong, J. P. Network elasticity of a model hydrogel as a function of swelling ratio: from shrinking to extreme swelling states. *Soft Matter* **2018**, *14*, 9693−9701.

https://doi.org/10.1021/acs.macromol.3c01253
Macromolecules XXXX, XXX, XXX−XXX